Hybrid Rocket Motor

A Senior Project

presented to

the Faculty of the Aerospace Engineering Department

California Polytechnic State University, San Luis Obispo

In Partial Fulfillment

of the Requirements for the Degree

Bachelor of Science

by

Zach Arena, Alexander Athougies, and Alden Rodulfo

June, 2010

Hybrid Rocket Motor

Zach Arena[1], Alex Athougies[2], and Alden Rodulfo[3]
California Polytechnic State University, San Luis Obispo, CA, 93407

Approved by

Dr. Dianne DeTurris[4]
California Polytechnic State University, San Luis Obispo, CA, 93407

This project involves the re-design, manufacturing, and testing of the Cal Poly Space System's 4th iteration of a M-class 98mm hybrid rocket motor. This motor utilizes hydroxyl-terminated polybutadiene as fuel with liquid nitrous oxide as the oxidizer. Modeling and analysis was conducted on a 12 port self-impinging swirl injector and fuel manufacturing to improve performance. Several hot and cold flow tests were conducted to validate the analysis and predict performance values. Test results included two test fires resulting in an average of 212 lb_f of thrust for 6 seconds with an I_{sp} of 160 seconds and an average thrust of 260 lb_f of thrust for 6 seconds with an I_{sp} of 200 seconds. Analytical models predicted a thrust of 225 lb_f for 6 seconds with an I_{sp} of 180 seconds.

Nomenclature

a	=	empirical regression constant
A	=	cross sectional area (in^2)
d	=	diameter (in)
F	=	force (lb_f)
g	=	gravitational acceleration (32.2 ft/sec^2)
G	=	area mass flux (lb_m/in^2–sec)
h	=	specific enthalpy (BTU/lb_m)
H	=	enthalpy (BTU)
HM	=	hybrid motor
I	=	impulse (lb_f-sec)
K	=	head loss coefficient
L	=	length (in)
m	=	mass (lb_m)
M	=	Mach number
n	=	empirical regression constant
N	=	number of some unit
OF	=	oxidizer to fuel mass ratio
P	=	pressure (psi_a)
r	=	regression rate (mm/s)
r	=	radius (in)
R	=	ideal gas constant
t	=	time (sec)

[1] Undergraduate Student, Aerospace Engineering Department, 1 Grand Avenue San Luis Obispo, CA, 93407, AIAA Student Member.
[2] Undergraduate Student, Aerospace Engineering Department, 1 Grand Avenue San Luis Obispo, CA, 93407, AIAA Student Member.
[3] Undergraduate Student, Aerospace Engineering Department, 1 Grand Avenue San Luis Obispo, CA, 93407, AIAA Student Member.
[4] Professor, Aerospace Engineering Department, 1 Grand Avenue San Luis Obispo, CA, 93407, AIAA Member.

T = temperature (ºR)
U = internal energy (BTU)
v = specific volume (in^3/lb$_m$)
v = velocity (in/sec)
$\cancel{V}$ = volume (in^3)
x = quality of vapor – liquid mixture (%)
ε = area expansion or contraction ratio
γ = ratio of specific heats
ρ = mass density (lb$_m$/in^3)
σ = stress (ksi)
τ = thickness (in)

Subscripts
1 = nozzle convergence or intake plane
2 = nozzle divergence
a = absolute
avg = average
Atm = atmosphere
b = related to combustion
C = current
Cg = combusted gases
Ch = combustion chamber
E = nozzle exit plane
f = fuel
f = force
Fo = formation
Free = open or inevitable
I = initial
In = inside measurement or of port
Inj = injector orifice
L = liquid
m = mass
Max = maximum
Noz = related to nozzle
ox = oxidizer
Out = outside measurement
Port = cylindrical burn surface in grain
R = reaction
sp = specific
S = stagnation
t = function of time
T = tank
Theo = theoretical
Th = nozzle throat
V = vapor

I. Introduction

THIS project is a student led, designed, and built M+ class (5120-10240 N-s total impulse) hybrid rocket motor. This motor is designed for air-start capability on the 2nd stage (sustainer) of a 2-stage rocket with the 98mm amateur rocket standard motor diameter in mind. While designing a rocket motor from the ground up poses several difficult challenges in itself with regards to pressures, temperatures, and mixture ratios, designing for air-start capability presents additional challenges to design and manufacturing that ground testing lacks. These challenges include weight, and size reductions while increasing the complexity of the control system. In order to use the system as a flight model all components must be small enough to fit within the maximum 6 inch diameter body tube of the rocket. Weight presents many challenges because the lab testing model requires additional strength to adequately ensure safety of the personnel testing the motor while the flight model must be light enough to ensure thrust to weight ratios promote stable flight. Also, when designing and building for flight one must also take into account the autonomous systems required to initiate and control the motor which are often cumbersome with large power requirements.

This hybrid motor utilizes liquid Nitrous Oxide (N_2O) as the oxidizer and Hydroxl-Terminated Polybutadeine (HTPB) as the fuel. The motor is designed to run at an oxidizer pressure of 600 psi and produce 300 lb_f of thrust using the self pressurization property of N_2O to maintain tank pressure. The current model is the 4th iteration of the motor, or HM4. The first model utilized commercial off-the-shelf hybrid rocket components, from RATTWORKS, such as polypropylene fuel grains and injectors. As experience was gained from HM2 and HM3, further customization and experimentation was done to improve performance and caused all major components of the motor to become student designed and built. Lessons learned from earlier component testing moved the project away from commercial injectors and towards machining custom injectors with the addition of low pressure water and N_2O flow tests being conducted prior to use in hot fire tests. For test fires, the motor is mounted horizontally on the test stand and uses a moment arm to transfer thrust to the load cell. The test stand is rated to 2500 lb_f of thrust to ensure adequate strength. It is secured using four turnbuckles and forged eye-bolts rated to 2200 lb_f each to distribute the load.

The current iteration, HM4, is the first configuration to use the Aerospace Department's new Propulsion Lab located in Building 41, Room 144. HM4 utilizes a portable control box designed for both ground and flight testing. The design has been improved to include a new high mass flow oxidizer feed system rated at 3000 psi_g complete with 1800 psi_g blow-off safety valves. In addition, a high mass flow Swagelok ball valve actuated with a 12V 212 in-lb (17.6 ft-lb) torque windshield wiper drive gear motor is being used, as well as a custom built 12 port self-impinging swirl injector, tank suspension weighing system, and graphite interchangeable nozzles. The current setup allows the supply tank to be wheeled into the lab and strapped to a support pole during filling procedures. Once the flight tank is filled, the filling assemblies can be disconnected and purged to allow removal of the supply tank from the test area during motor test fires. A schematic of the hybrid test setup is shown in Figure 1.

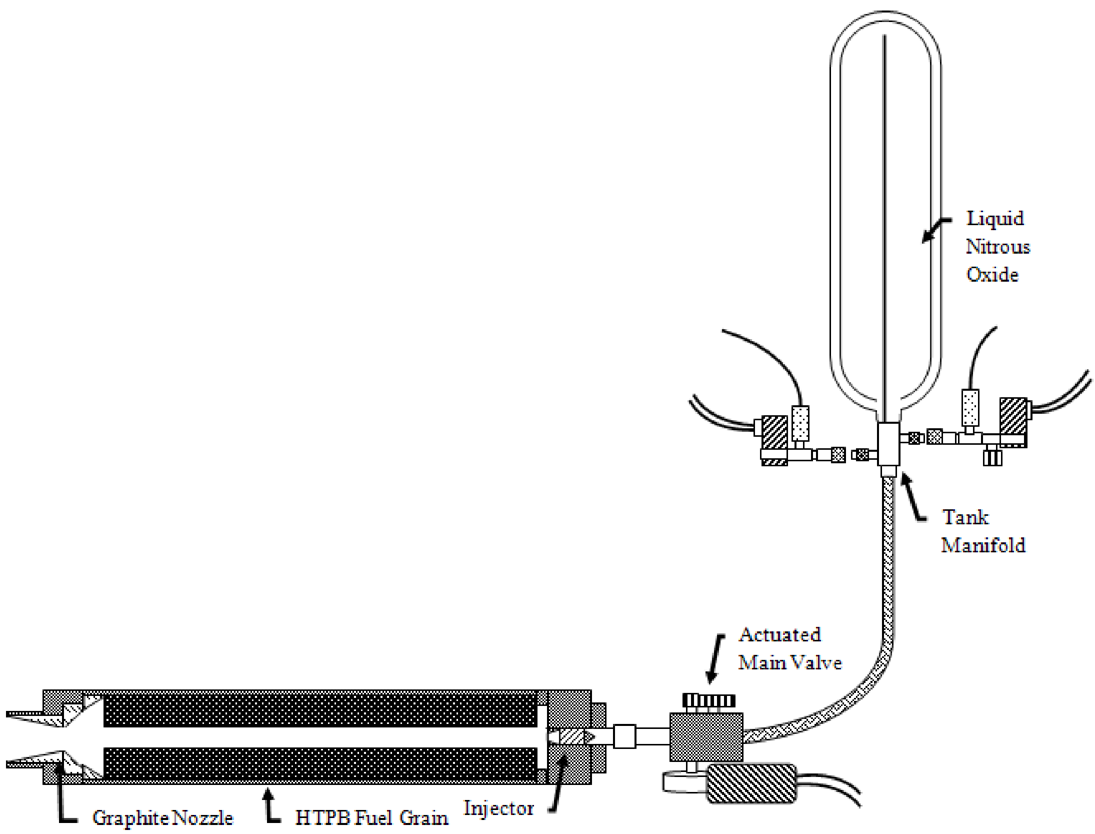

Figure 1. Hybrid Test Setup

II. Motor Design

A. Oxidizer System

The oxidizer feed system consists of 4 main components. The flight tank is a commercially sourced Kevlar wrapped Aluminum tank rated for gaseous oxygen. The tank manifold connects the tank to the fill, vent and motor feed assemblies in addition to safety and sensor systems. A steel braided flexible line delivers oxidizer to the main valve which controls flow rate into the injector.

1. Tank Manifold

The tank manifold design serves three purposes: to deliver oxidizer from the flight tank to the main valve, to provide the means of filling the flight tank from the supply tank, and to release pressure in the system in case of an oxidizer over pressurization. The tank manifold must also withstand the high pressure oxidizer ranges from 600 psi_g to 800 psi_g. The main purpose of the tank manifold is to deliver oxidizer from the flight tank to the main valve; to accomplish this the flow path between the tank and the main valve needs to remain unrestricted to ensure that the cryogenic liquid oxidizer remains a liquid until it reaches the injector. Area change and connections within the flow path must be minimized to reduce the opportunity for tripped flow. To satisfy these requirements, a crescent shaped opening in the tank manifold is used. This crescent shaped opening maximizes the area at the tank end and also allows for a smaller secondary hole containing a siphon tube allowing air and gaseous nitrous oxide to escape through a vent during the filing process. The tank orifice is 0.73 inches in diameter and the main valve has an inner diameter of 0.5 inches. The crescent shaped hole used on the tank side of the manifold fits inside the 0.73 inch diameter tank opening and then opens up to a 0.5 inch inner diameter to match the valve orifice. The transition between the crescent opening and the 0.5 inch diameter opening occurs within the tank manifold where the area change between them is minimized to a 20% difference. This minimal area change ensures that the cryogenic oxidizer does not expand rapidly inside the piping causing a phase change from its liquid state to its gaseous state. Also by manufacturing the tank manifold as one piece the tank manifold is used as the only link between the flight tank and the main valve; this direct connection reduces the weight of the motor and also reduces the number of connections in the piping ensuring that there are few trip points to keep the flow of oxidizer smooth.

The tank manifold also provides the means of filling the flight tank with oxidizer from an external supply tank. To accomplish this task the tank manifold needs two additional flow paths. The first flow path provides a connection to the flight tank from an external supply tank; this connection merges directly with the flow path from the flight tank to the main valve. The second flow path merges with the siphon tube located at the tank end of the manifold; this flow path allows air and gaseous oxidizer to escape from the tank allowing liquid oxidizer to fill into the flight tank. A 3000 psi self closing quick disconnect valve is used to close these external connections .

The third purpose of the tank manifold is to release excess pressure in the system in the event that the liquid oxidizer gets too hot and over pressurizes the system. For this a smaller flow path is used that merges with the main flow path connecting the tank and the main valve. This connection is threaded and a burst cap rated to burst at 1800 psi is used as the pressure relief system. If the system exceeds 1800 psi the burst cap will rupture and release the contents of the flight tank and feed system to atmosphere.

The tank manifold is manufactured from a single piece of 1.5 inch in diameter hexagonal brass bar stock. The first step in manufacturing is to cut the stock and face both sides of the brass bar in a lathe to approximately 2.8 inches in length. The tank end of the tank manifold is then turned down to 0.75 inches in diameter where a 3/4 – 16 die is used to cut threads. While turning, the initial rounding operation must be done with care and at a low feed rate to prevent chattering and vibrations which will eliminate any accuracy in the machine. On the main valve end of the tank manifold the diameter is turned to 0.84 inches in diameter and a 1/2 – 18 NPT die is used to create the threads. To create the crescent shaped hole on the tank end of the manifold, the piece is placed into a computer numerically controlled (CNC) mill where a straight 1/4 inch end mill tool is used to remove the material. The straight 1/4 inch end mill is needed because the flutes of the tool are the same diameter as the held end of the tool; this allows the end mill to penetrate into the brass further than a standard end mill. The crescent shape hole is then milled 1.5 inches deep from the tank end of the manifold. At the main valve end of the tank manifold a 0.5 inch diameter drill is used and will merge with the crescent shaped hole from the other side of the manifold. Also, at the tank end of the manifold a smaller hole is drilled using a #24 drill where the siphon tube is inserted; this hole is drilled to a depth of 1.25 inches. On the same side as the dip tube but perpendicular to the hole, another hole is drilled using a 7/16 inch diameter bit and finished with a flat end mill of the same diameter. This hole is drilled only until the siphone tube hole is visible. Another 7/16 inch in diameter hole is also drilled on the opposite side of the tank manifold which is perpendicular to the crescent shaped hole that was made earlier. This hole is drilled until it merges with the main flow path between the tank end of the manifold and the main valve end of the manifold. Both 7/16 holes are then tapped using a 1/4 NPT bottoming tap. The last hole is used for the burst cap; this hole is a 3/16 hole with and tapped with a 3/16 – 24 tap. Since the burst disk requires a seat the hole must not be drilled as a through hole; a through hole into to the flow path must be of a smaller diameter. The burst disk is then screwed into this hole. Figure 2 shows the construction diagram of the tank manifold. To ensure that the tank manifold is able to withstand the pressures of the liquid oxidizer a finite element analysis model was created to show the major stress points of the manifold under pressure. Figure 3 shows the finite element analysis (FEA) model of the tank manifold and illustrates that the tank manifold can withstand a pressure above 3000 psi_g.The FEA model is tested using CosmosWorks embedded into SolidWorks[5]. Material properties are taken from Military Handbook #5.

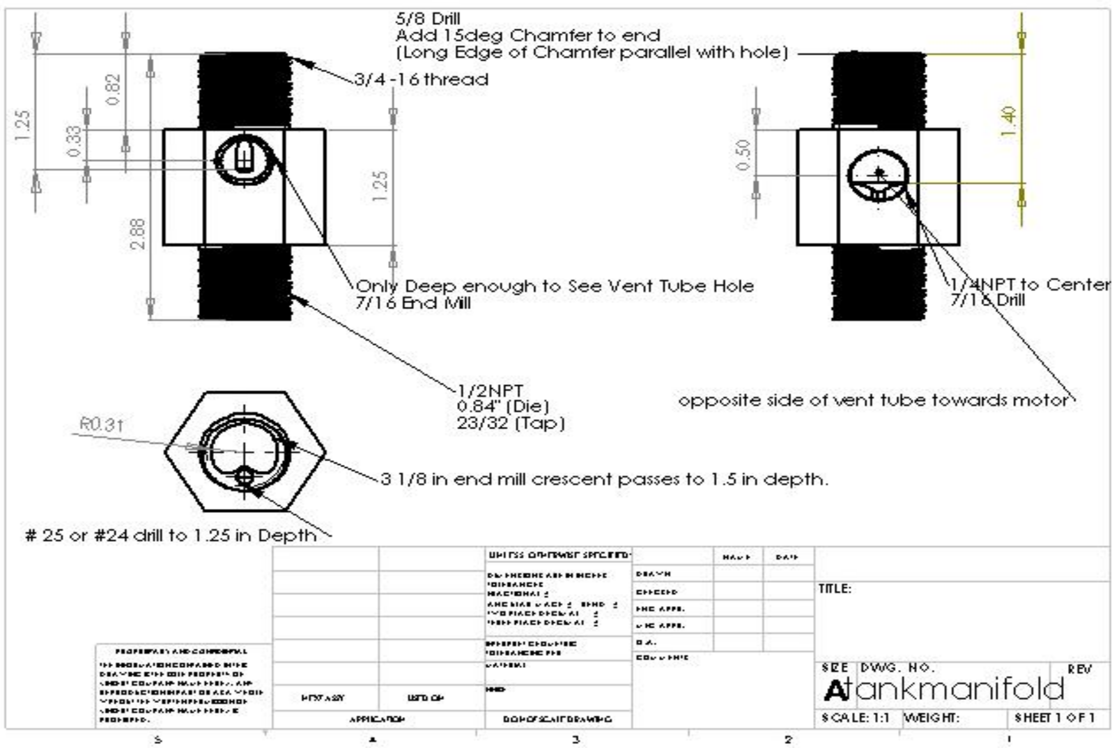

Figure 2: Construction Diagram of Tank Manifold

[5] (Dassualt Systemes SolidWorks Corporation n.d.)

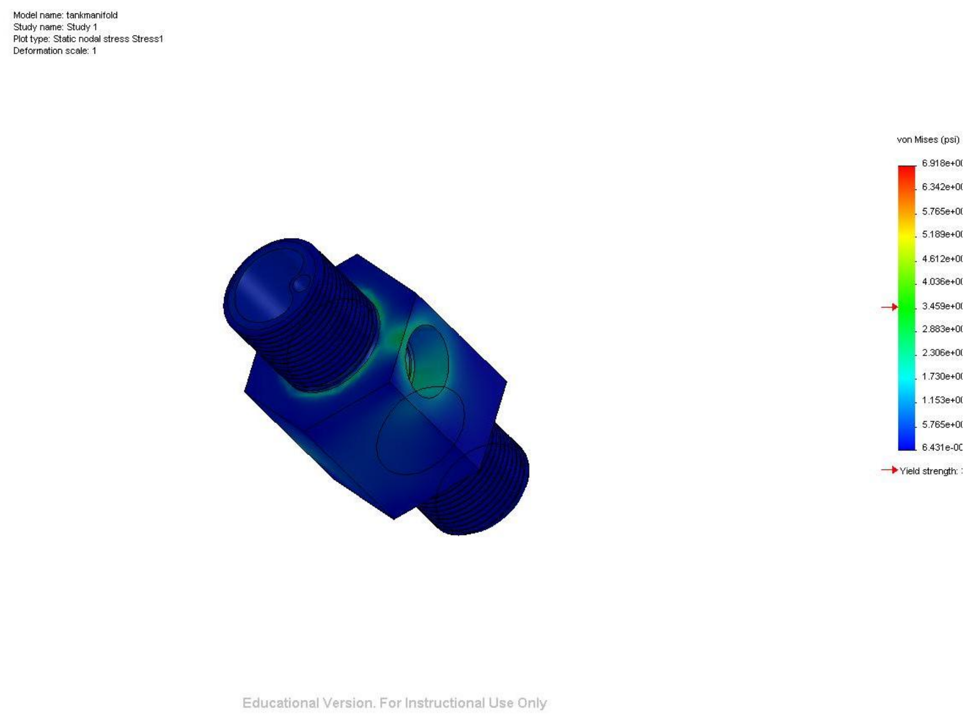

Figure 3: Finite Element Analysis Model of the Tank Manifold

2. Main Valve & Feed Assembly

The purpose of the main valve is to provide the means of controlling the flow of oxidizer into the combustion chamber. This valve is crucial to the operation of the motor and must have high reliablity; the valve must also withstand and operate at the high pressure and extreme temperatures of liquid nitrous oxide. This valve must be operated remotely and therefore it was decided that an electronically controlled valve is required. The first type of valves that were looked at were electronically controlled solenoid valves; solenoid valves use a diaphragm that is electro-magnetically controlled. The flow inside most solenoid valves is diverted multiple times in order for the diaphragm to stop the flow. First the inlet of the solenoid valve diverts upward into the piston chamber that holds the diaphragm. The flow is then diverted 180 degrees downward into the exit of the piston chamber. Once the flow exits the piston chamber it is diverted 90 degrees once more before exiting the valve. Since the flow inside of a solenoid valve is diverted multiple times, the cryogenic oxidizer moving at fast velocities through the valve would undergo a phase change which is not ideal.

Another disadvantage of using solenoid valves is the valve orifice sizes. The injector has an inner diameter of 0.5 inches and the exit of the tank manifold has an inner diameter of 0.5 inches as well. Solenoid valves have very small orifice sizes in order to withstand high pressures; the higher the pressure that the solenoid valve can handle the smaller the orifice is within the valve. The small orifice sizes inside solenoid valves create a restriction of flow within the system that reduces the mass flow rate. For a motor that requires an oxidizer mass flow rate of about 1 lb_m per sec this is an unfavorable condition. Another major disadvantage of using solenoid valves involves the diaphragm and piston. When the diaphragm and piston are exposed to low temperatures they can freeze and get stuck. This reduces the reliability of the valve and becomes a safety hazard. With all the disadvantages of using solenoid valves it was concluded that solenoid valves are not a viable option for the main valve.

The next option considered was an electromechanically controlled ball valve. However, most commercial electromechanically actuated servo valves are too large and heavy. They are are very bulky and do not fit within the 6 inch body diameter of our rocket and therefore a custom mechanism was required.

The first step in designing the servo valve was to find the ball valve that could withstand and operate under high pressures and extreme temperatures. A ball valve was chosen because the valve orifice is the same diameter as the inlet and outlet of the valve allowing for maximum flow rate through the valve. Also, ball valves allow for axial flow through the valve and therefore do not restrict the flowing fluid; the ball valve chosen was custom ordered from

Swagelok. A stainless steel valve was chosen to withstand the high pressures of the oxidizer and prevent corrosion. The valve seats were constructed of PEEK or PTFE to ensure that the oxidizer does not erode the seating surface. The valve stem was designed with compression spring washers, called a live loaded packing system, allowing automatic self-adjustment when exposed to extreme temperatures. The valve chosen with all of the criteria listed above is the Swagelok SS-45TF8 shown in Figure 4.

Figure 4: Swagelok SS-45TF8 stainless steel live loaded ball valve

The next step was to find a mechanical actuator to open and close the valve. Since the valve is live loaded the amount of torque required to actuate it ranges from 8 foot pounds to 9.5 foot pounds of torque depending if the valve is under pressure or not. The best means of opening the valve, without relying on pyrotechnics, is a motor. The motor would have to provide the torque required to open and close the valve while it is under pressure and must be able to open and close the valve within one second. To provide the torque to actuate the valve two gear systems were used to increase the amount of torque at the valve stem. The first gear reduction occurs at the motor; the motor utilizes a worm gear and pinion to reduce the speed of the motor and increase the torque. The output shaft of the motor then turns another pinion gear which is then attached to the spur gear at a 3:1 reduction ratio. This reduction ratio increases the torque of the motor and reduces the speed of the motor by a multiple of 3. By using these gears the motor is able to output 16 foot pounds of torque to the valve stem and open and close the valve within 0.45 seconds. The gears were bought from McMaster – Carr and the motor used is an AME 218 series 12 volt long shaft gear motor shown in Figure 5.

Figure 5: AME 218 series 12 volt long shaft gear motor used to actuate the ball valve

The last step in the design of the main valve assembly was to house the entire assembly together into one piece. A rigid mounting plate is required to withstand the torques exerted by the motor. Also, the configuration of the gears, the valve, the motor, and the limit switches had to be held together under very tight clearances in order for the valve to function properly; to accomplish this task a base plate was constructed that would hold the valve and the motor securely in place. To ensure the base plate and the top plates are within tolerance both pieces were CNC machined. The valve is secured into the base plate using two U-bolts, and the motor is held onto the base plate with screws mounted on the motor's gear head assembly. With the motor and valve secured in place,,a top plate is used to guide the shaft of the motor to prevent the gears from slipping and to hold the limit switches that tell the motor to stop when the valve is in the fully open or fully closed position. The pinion gear is set onto the motor shaft using a set screw and the spur gear mounted on the valve is set using a notch and key; the top and bottom plates are then held together using screws. Figure 6 shows a front and top view of the complete valve assembly. The motor is placed such that that the U-bolts holding the valve are easily accessible and the motor body is parallel to the flow path of the valve. By making the body of the motor parallel with the flow path of the valve the whole assembly can be fit inside of a 6 inch diameter rocket; in particular, 'Caution: Flammable', a rocket built and test flown by Cal Poly Space Systems. Figure 7 shows a construction diagram of the base mounting plate as well as the top plate.

When machining the mounting plate be sure to check that the tools fit the part. For example, when countersinking the screw clearance holes for motor attachment it is necessary to have a tool and chuck combination which can get into the grooves of the base plate without hitting the walls; you may find that this operation is best done on a drill press. In order to maintain tool clearance with the part while cutting the deep grooves you may opt to only grip a minimum of 0.06 inches. This is enough grip-surface as long as feed rates are held low. Use caution and take your time as these parts require quite a bit of material removal.

A stainless steel braided hose connects the tank manifold to the inlet of the main valve. This PTFE stainless steel braided hose has an inner diameter of 0.5 inches and has a 1/2 inch NPT male connection at each end. The hose is needed to bridge the gap between the vertical flight tank and the horizontal chamber. The length was chosen to match the test configuration; any looping or slack in the line could lead to kinking or other adverse flow effects. The hose is rated to 1500 psi with a burst factor of 3.

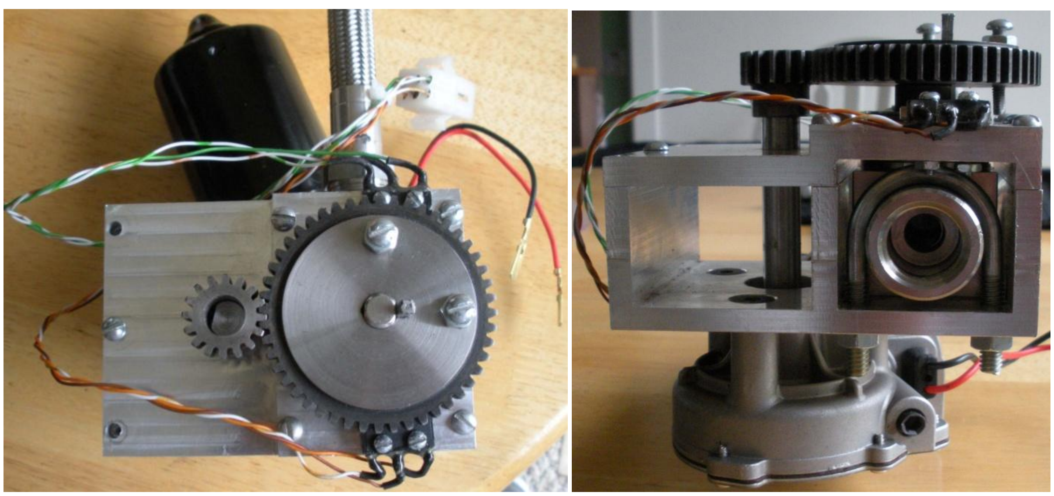

Figure 6: Top and front view of the completed main valve assembly

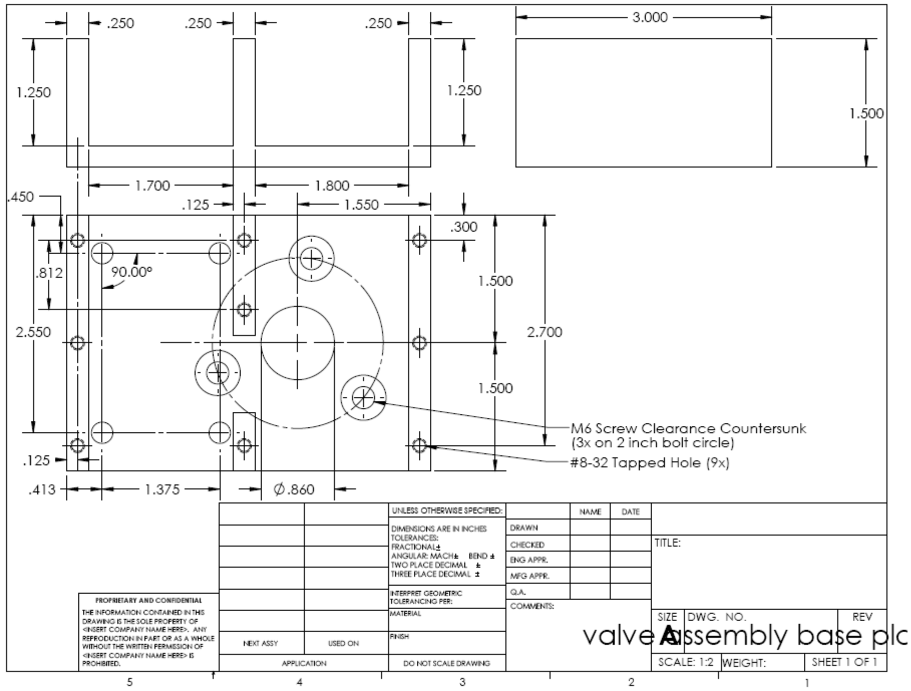

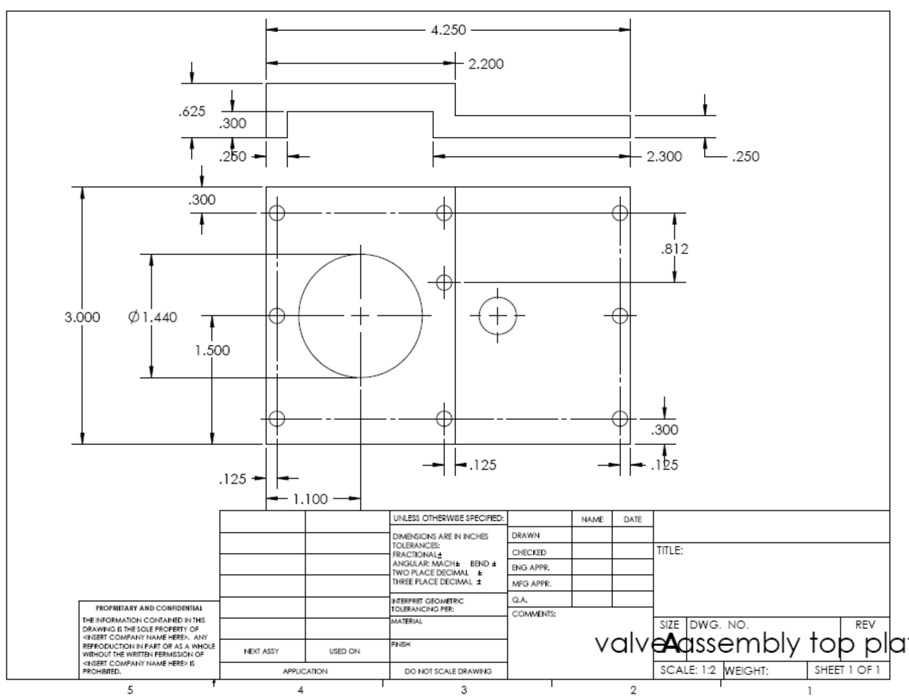

Figure 7: Construction diagrams of both the base plate and the top plate of the main valve assembly

3. Injection Manifold

The injection manifold serves three purposes. Its first purpose is to atomize the liquid oxidizer into small droplets. Its second purpose is to deliver oxidizer into the combustion chamber at the predicted required mass flow rate of between 0.8 and 1 lb_m/sec. The last task of the injector manifold is to swirl the oxidizer inside of the combustion chamber to promote mixing with the fuel.

A series of experiments were conducted with water to visually observe the flow properties of different injector configurations and to test their atomization properties. The first experiment conducted was to test the atomization properties of having a secondary flow impinge on a primary flow. In order to conduct this experiment an injector was crafted from a piece of wood that contained two separate flow paths. Figure 8 shows a model of the simple injector used for the experiment; each flow path contained a valve so the effects of each flow could be seen independently.

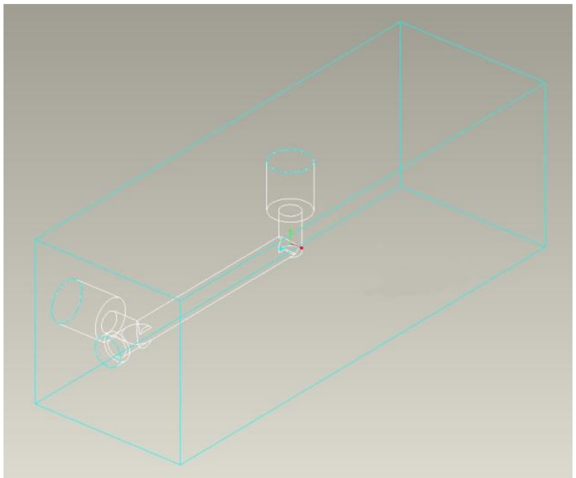

Figure 8: The injector design for the primary and secondary flow atomization experiment

The first step of the experiment was to turn on the primary flow through the injector and analyze the flow pattern and the atomization characteristics. With the primary flow turned on, the flow pattern shows a single stream of liquid flowing out of the injector as seen in Figure 9. This single stream of fluid shows very little atomization of the fluid as expected.

Figure 9: The injector flow pattern and atomization characteristics with only the primary flow active

When the secondary flow valve is opened, the secondary flow impinges against the primary flow and atomizes the liquid. This atomization is seen in Figure 10 where there aren't any visible solid streams of fluid exiting the injector. Also, the flow pattern with both the primary and secondary flows active shows a more conical shaped spray pattern.

Figure 10: The injector flow pattern and atomization characteristics with the primary and secondary flows active

This experiment proves that impinging a secondary flow onto a primary flow results in better atomization of the fluid. The next step in the development of the injector was to find a way to split the fluid flow from a single flow path coming from the main valve into multiple flow paths that can be redirected at different angles. A cone was used at the inlet end of the injector for the second injector experiment. This cone diverted the incoming flow outward at a 45 degree angle then channeled the single flow path into 6 separate flows. These 6 flow paths are then redirected 90 degrees inward towards the center of the injector. Once the flows converge at the center of the injector all 6 flows impinge in each other atomizing the fluid. The second injector was constructed using extruded aluminum and was made of two pieces as shown in Figure 11. The test results showed very good atomization and the injector produced an outward spraying flow pattern as shown in Figure 12. Using computational fluid dynamics (CFD), a flow model was created to verify the test results. Figure 13 shows the flow pattern created by the CFD model which shows similar flow results as the experiment. The model was created using SolidWorks[6]. Water was used as an analogous fluid. Pressure differences are kept within city water pressure limits for verification purposes.

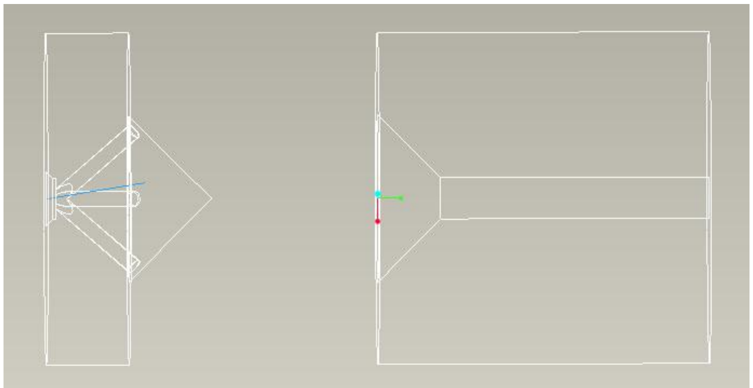

Figure 11: The second injector using a cone to divert the single flow into multiple flow paths

[6] (Dassualt Systemes SolidWorks Corporation n.d.)

Figure 12: The second injector water test proving that impinging flows improve atomization and create an outward spray pattern

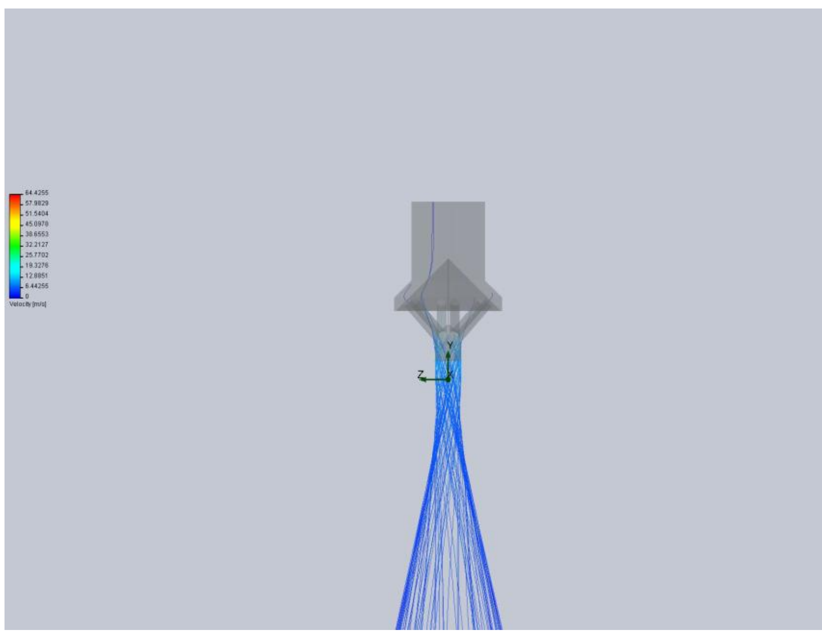

Figure 13: CFD results for the second injector experiment

The next step was to design the full scale flight injector. The flight injector would combine the principles of the previous injectors along with an external cup to induce a swirl on the fluid. The injector utilized a cone inlet which diverted the single incoming flow into 12 separate flow paths. These flow paths were then diverted axially at the angles of 20 and 40 degrees. The 20 degree holes were considered as the primary flow and the 40 degree holes were considered as the secondary flow. The 12 separate flow paths were paired up to form 6 independent primary and secondary flows that impinged at the base of the cup. The purpose of the cup is to induce a swirl on the atomized fluid and to cause a phase change in the cryogenic liquid oxidizer. Once the primary and secondary flow of oxidizer interacts with each other the fluid atomizes and interacts with the base of the cup at an angle of 30 degrees. The fluid is then forced to follow the rim of the cup where it is forced to swirl in an axial direction. By swirling the oxidizer in the combustion chamber the combustion chamber length is effectively lengthened increasing the efficiency of combustion. A center cone at the exit of the injector was added in order to force the outgoing fluid towards the walls of the combustion chamber. The mixing ability of the fuel and oxidizer is increased by forcing the fluid outward towards the fuel grain. Before the actual injector was manufactured, a CFD model was created to analyze the flow pattern. Figure 14 shows the results of the CFD model which provided the desired flow pattern of the fluid exiting the injector. The CFD model, Figure 14, shows a low pressure region created by the impinging flow at the base of the cup; this low pressure region aids in the phase change of the oxidizer from a liquid to a gas which is ideal.

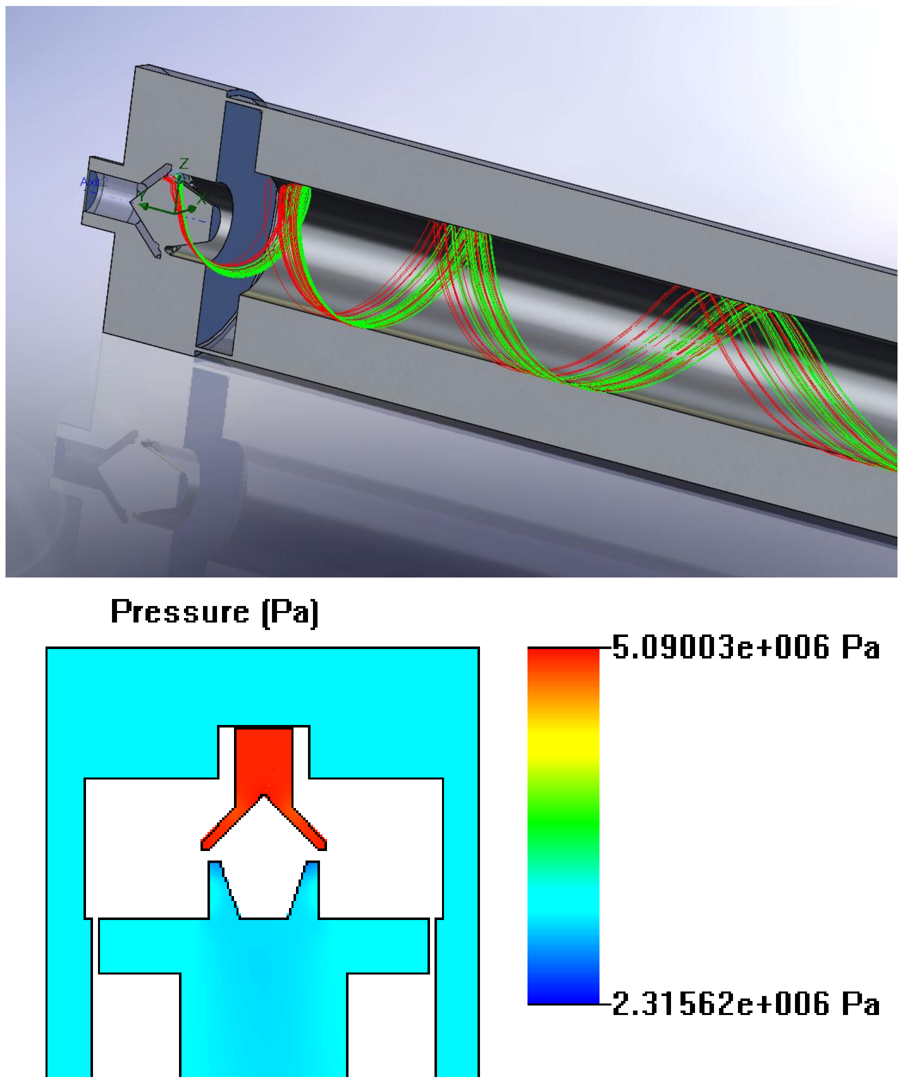

Figure 14: The CFD test results of the flight injector where the top shows the flow pattern of one pair of injection ports and the bottom shows the pressure inside of the injector

The injector was constructed using 3 pieces of extruded 6061 aluminum. The inlet piece of the injector connects to the main valve and is screwed into the outlet piece of the injector by 5 screws in a bolt circle. A PTFE O-Ring is used to seal the two pieces together and prevent leaks. The inlet side of the injector has 1/2 inch NPT male threads at one end and the exterior cone section of the injector. The outlet piece of the injector has the inner cone section that diverts the flow of fluid outward as well as the 12 ports that expel the fluid into the cup and into the combustion chamber. The screws are tightened in a star pattern. The third piece of the injector is the center cone at the outlet side of the injector which helps guide the fluid outward towards the fuel grain; this center cone is held in place by a screw. During hot fire tests this center cone melted away; further experimentation requires the use of graphite or more exotic metals with high melting temperatures. Figure 15 shows the construction diagram of the outlet injector piece.

The inlet piece of the injector and the center cone are easily constructed by even a novice machinist, however the main body of the injector is the most difficult. This piece was designed with a specific process in mind. The main stock is CNC lathed and milled, as shown in Figure 16, to form a boss which includes most features except the cone;

the piece is a 2 inch extrusion at this point, the angled injector holes and threads (codes number 440 and 441 on the Haas VF2 in Mustang ’60 for a stock length of 1.7 inches). The next step is to chuck the piece on the to-be cone extrusion and add the threads which will connect to the casing. Next flip the part over and chuck on the 0.25 inch recession, added for this specific purpose, and turn the center cone. It is suggested to use a boring bar and spinning the part in reverse, as shown in Figure 18; this is a point of no return. If any repairs must be done on the threads a new part is recommended. The next steps are done on a mill with a rotary table attachment. The mill head needs to be angled therefore the manual knee mill is recommended such as the Bridgeport or Ganesh in the ME Special Projects Lab. Due to clearance issues use the method noted in the Appendix.

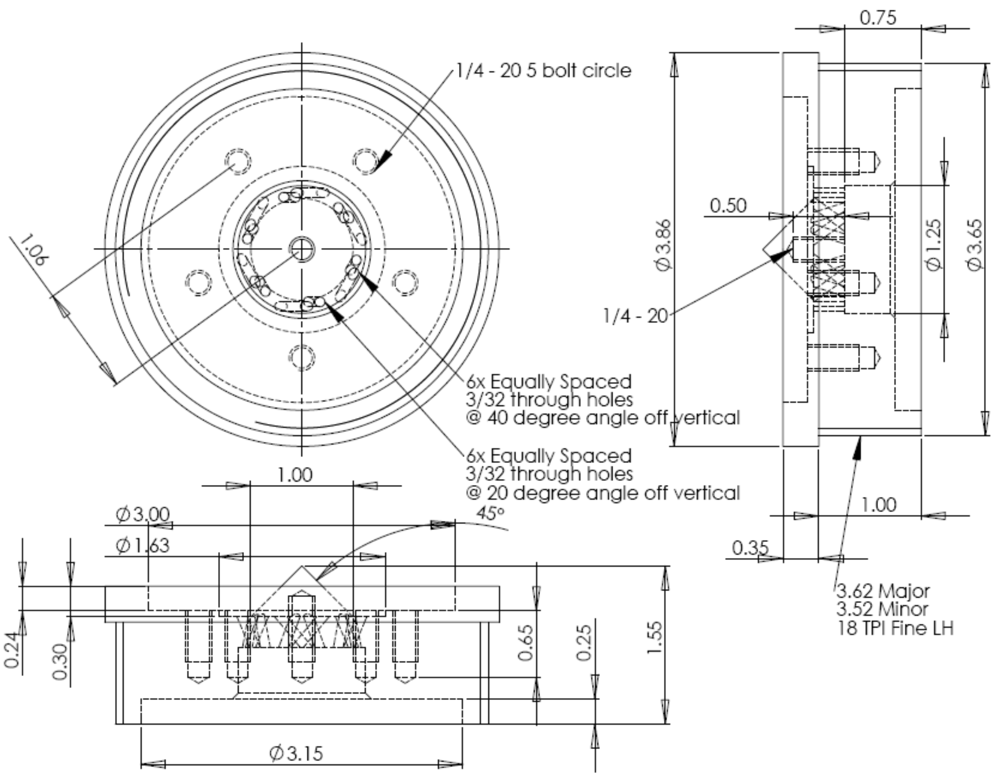

Figure 15. Construction Drawing of Injector

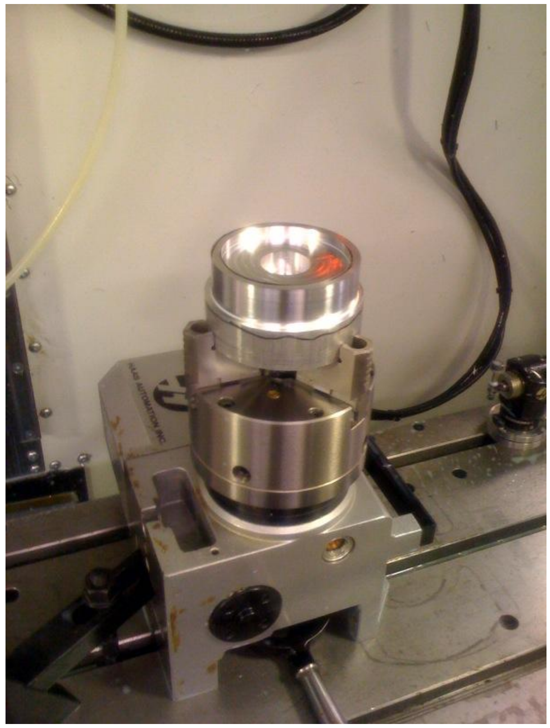

Figure 16. Injector Blank in process on HAAS VF2 Mill at Mustang '60 Machine Shop

Figure 17. Method for Drilling Angled Holes in Aero Hangar Machine Shop

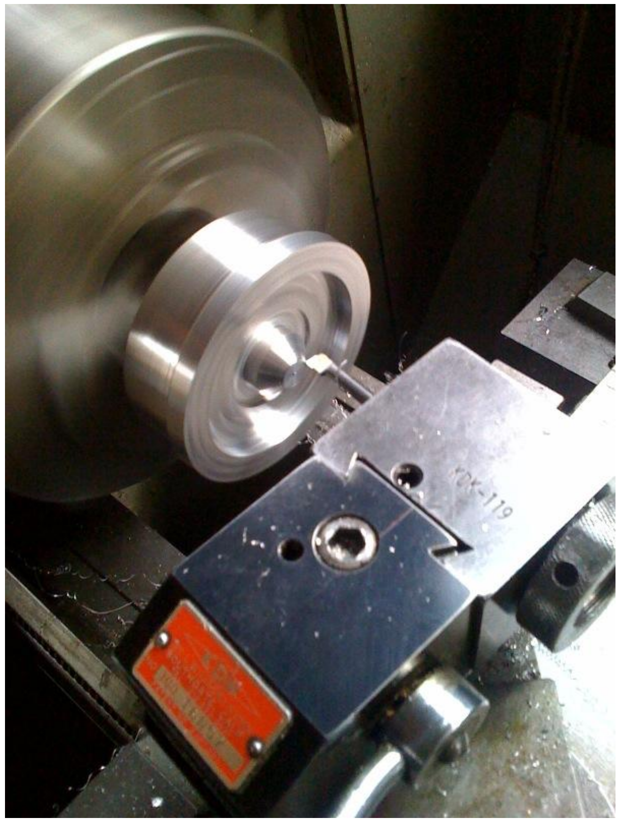

Figure 18. Machining Setup for Flow Control Cone on Injection Manifold
(Note: Part spun in reverse and chucked from the inside out)

B. Combustion Chamber

The combustion chamber, motor casing, is a vital part in the safety and performance of the hybrid rocket motor. Unlike solid or liquid rocket engines the thermal gradient along the length of the chamber can vary greatly; this fact is perceivable immediately following a test fire. The injector side of the motor is only warm to the touch but the nozzle side of the chamber is capable of flash boiling drops of water. Nevertheless, the chamber must be capable of withstanding 3000 psi_a of static pressure with a burst factor of 3 at qualification level loads. At the same time it must follow the Tripoli Rocketry Safety codes[7] outlining specific material requirements and it must fit in standard 98 mm amateur rocket style motor mounts.

Based on the requirements above, the casing is made of 6061-T6 aluminum shown in Figure 19. End caps are held on by threads which maintain constant load paths rather than dual radial bolt circles more readily seen in large amateur solid rocket motor development; these develop stress points at the screw locations shown in Figure 20. The lack of stress concentrations allows for analysis to remain primarily analytical rather than requiring advanced methods such as FEA. This also allows the casing to remain thinner to reduce weight. Aluminum 6061-T6 has a yield tensile stress of 40 ksi[8]. Equation 1 (Beer, Johnston and DeWolf 2006) allows us to determine the casing thickness based on hoop stress for a thin wall cylinder.

$$\frac{\quad}{\quad} \tag{1}$$

The minimum thickness for the casing is 0.3940 inches; this thickness applies in particular to the thread portions of the casing since they are the thinnest. However within our thickness constraints of 0.25 inches a maximum burst factor of only 1.90 can be achieved, based on this burst factor the minimum thickness must be

[7] (Tripoli Rocketry Association n.d.)
[8] (American Society of Metals 1990)

larger than 0.131 inches. In order for a burst factor of 3 to be retained the internal pressure must be held under 1900 psi_g. The burst cap safety valve triggers at 1800 psi_g, allowing a 5.6 % margin.

This lower burst factor can result in large deflections in the casing radius when fully pressurized allowing some blow-by of the seals. No blow-by has been experienced in the past and the seals followed precedent; however the higher pressures experienced in testing showed that a new sealing method must be developed. The standard sealing method consists of o-rings tightened to compress against the fuel.

The casing of HM3 was chosen for the first test fires since it had already been proven to hold combustion pressure during previous test fires. Unfortunately due to an error in manufacturing it had a right-handed thread on one side and a left-handed thread on the other; in addition both threads had different minor and major diameters. Although the different thread directions were a pure mistake on the part of the former student who built it, the reason for the different diameters is unknown. Both threads are cut at 18TPI; this pitch gives the required grip area and shear allowance to withstand combustion pressure.

Due to failure of the HM3 during the first test fire, a new casing was manufactured; the new casing is built shorter to fit three 4.5 inch long grains. Since the end caps were already threaded when the new casing was made it was decided to keep the awkward threads even though a complete rebuild of the motor would have been beneficial. A decision to rebuild all of the components would have put the project severely behind schedule and testing would be further delayed.

Care was taken during the manufacturing process; a steady rest and a well centered lathe chuck shown in Figure 21 were used. The part was not turned faster than 100 rpm when using the steady rest to avoid the harmonics of the tube. Internal threads were cut using a boring bar ground to the required 30 degree cut angle. Each cut was verified twice to ensure precise machining; particular care was taken on the threads because interfaces between parts can cause damage and fit issues to multiple parts.

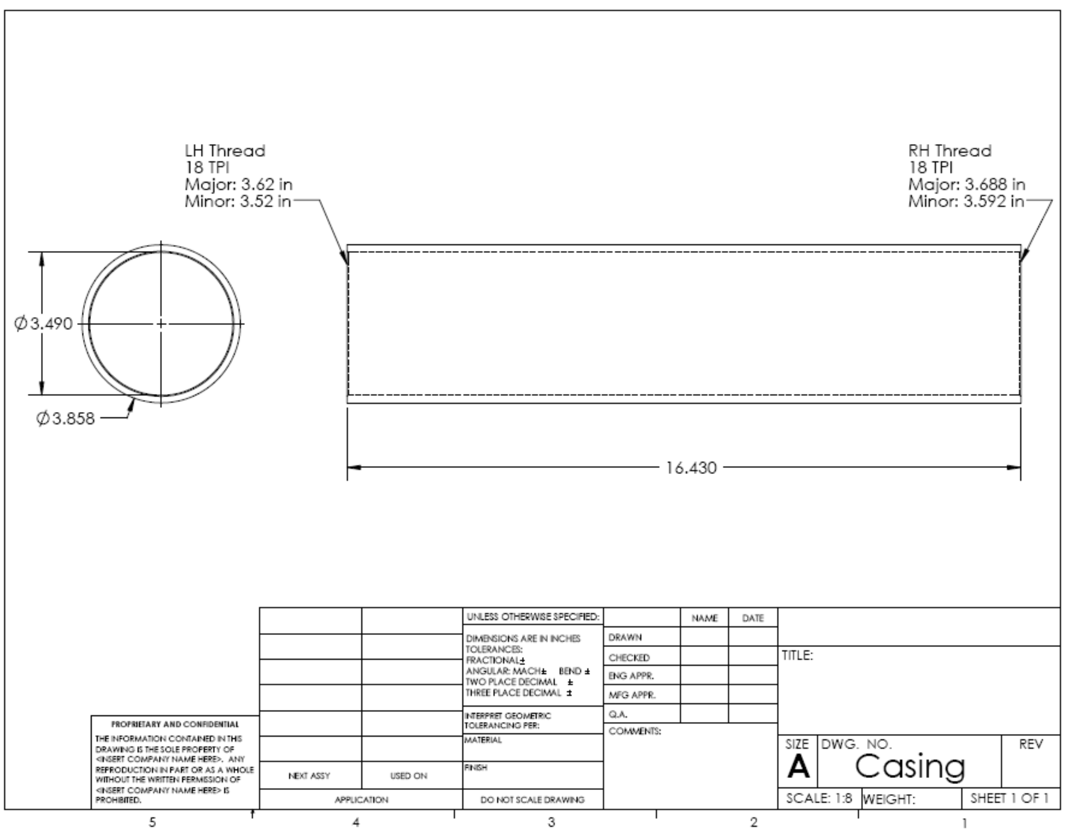

Figure 19: Casing Construction Drawing

Figure 20: Radial Bolt Style End Cap Retention (Nakka n.d.)

Figure 21: Casing Blank Mounted on Lathe

C. Nozzle

The nozzle is designed for three criteria: easy reconfiguration for a variety of tests, flight readiness, and low cost. Material for the nozzle, the throat in particular, was the most difficult to determine. The nozzle had to withstand temperatures estimated past 3000 degrees Rankine and flow velocities above Mach 3. These two requirements influenced materials choices towards metals such as Inconel. Unfortunately no steel can be used in the construction of an amateur rocket motor as per the Tripoli Rocketry Association Safety code[9]; chromium-molybdenum based steel and graphite have been used in the past for ground testing. Industry contacts suggested silica impregnated cast

[9] (Tripoli Rocketry Association 2010)

phenolic nozzles from a commercial supplier; while these seemed like a trivial solution they turned out to be rather expensive and had a low variety of geometries and throat diameters for our size of rocket motor.

The decision was made to use graphite as the nozzle material. While erosion is an issue with graphite, the ease of manufacturing, the thermal properties, and the readily available stock material favored the decision. A two piece nozzle design meant that a minimal amount of graphite dust is created in manufacturing and stock material costs are reduced. Sealing the two graphite pieces together posed a difficult problem at first since precedent warranted the use of lithium grease as the primary gap sealer. A labyrinth seal and press-fit components were the solution that provided the simplest manufacturing and simple integration of components. An industry contact recommended the use of RTV adhesive silicone sealant; at first this recommendation seemed eccentric since RTV silicone is flammable and has a melting temperature less than 1000 degrees Fahrenheit. Despite these facts the sealant was used and the labyrinth seal was removed. The results in the second test fire revealed that the sealant is remarkable in its ability to adhere and seal gaps even when exposed to temperatures in excess of 4000 degrees Rankine and Mach 0.8 gas flows. White lithium grease is used elsewhere to facilitate assembly, disassembly, and prevent residue build up in places such as the threads. Automotive gasket material is planned for future sealant material following the same technique of compression against the fuel grain. The material is expected to reduce burning which occurs at the top and bottom of the grain as well as providing a larger seal radial thickness reducing gas penetration and preventing gas-to-casing contact.

An initial throat diameter of 0.75 inches was chosen based on data from previous analysis on HM3 and steady state analysis using isentropic flow equations from Sutton[10]. The expansion ratio of 5.2 was determined through the same isentropic steady state equations for an average chamber pressure of 450 psi_a. This combination is designed to produce near optimum sea level thrust at that steady state condition; for HM4 this should be about midway through the burn. Radii of curvature for rounded or parabolic faces are derived as a function of throat radius using empirical data from Huzel[11].

Codes on the HAAS VF2 machine, # 518 and # 519, in the Mustang '60 shop were used to remove a majority of the material from a 4 inch extruded rod, 2.5 inch long billet. At this point the piece only required cleaning and threads. In addition the VF2 machine with the rotary table installed can break tools during a tool change since the machine will bring the tool holders down to the rotary table height. Use of the 'G54 G00 X-12' code before each tool change, or 'T' command', was used in order to move the table out of the way. The part was made with a 3 flute, 0.25 inch diameter carbide flat end mill running at 10000 rpm; a feed rate of 25 to 50 inches per minute (XY axis) and 0.05 to 0.1 depth of cut was used with plenty of coolant. The recess cut on the chamber side was used to grip the nozzle in a chuck once the threads were cut to avoid gripping the threads themselves. Due to the relative fineness of the threads care must be taken when machining them. Depths of cuts were limited to 0.002 to 0.005 inches. These are the same 'speeds and feeds' and tools that should be used on the injector CNC operations.

A vacuum cleaner was used when cutting graphite to suck in debris as it came off the part. This operation required two people; each person was equipped with safety equipment as demonstrated in Figure 25. Graphite is also very brittle so care was taken not to over tighten any clamp or jaws. As the part was bored through it grew weaker so the jaws were loosened accordingly. Graphite can be spun fast and endure a large depth of cut so long as centrifugal forces are satisfied and the cutting tool is very sharp with a large rake angle. The 4 inch diameter graphite was never spun faster than 1500 rpm particularly when it was bored out. Special care was taken to ensure a centered chuck; failure to do so would cause the part to shatter due to vibrations.

[10] (Sutton and Biblarz 2001)
[11] (Huzel and Huang 1992)

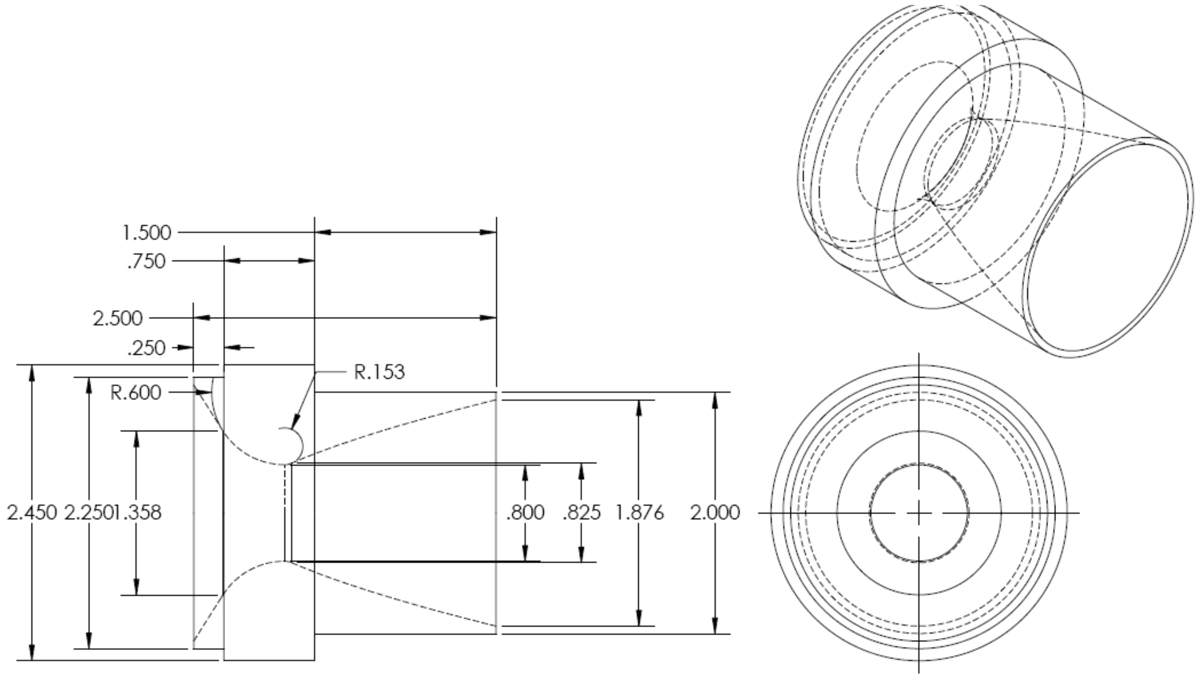

Figure 22: Construction Drawing of Graphite Throat Section (2nd Test Fire Dimensions)

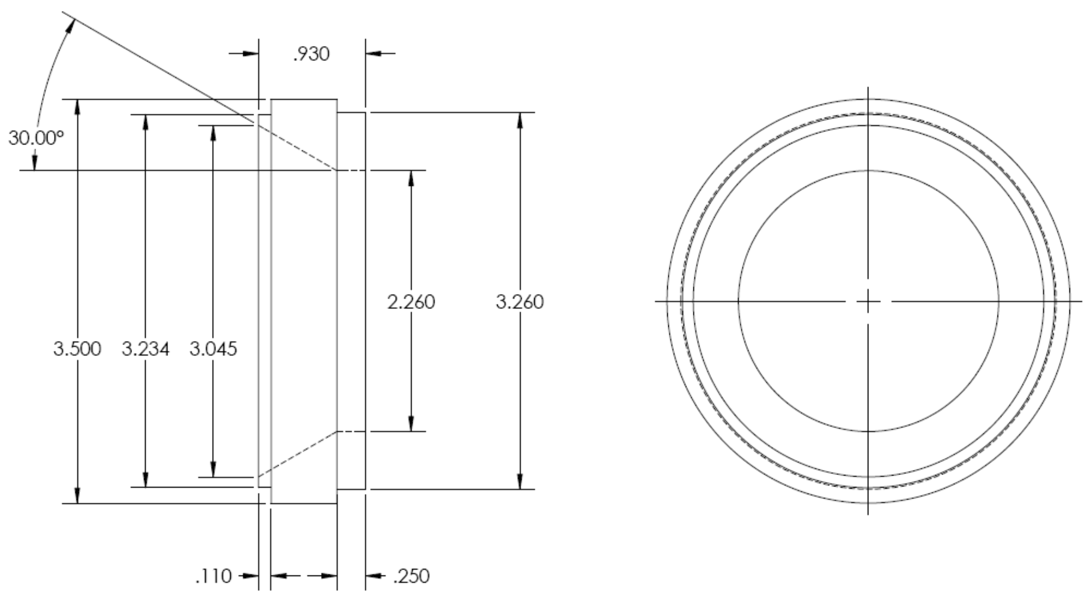

Figure 23: Construction Drawing of Graphite Convergence Section

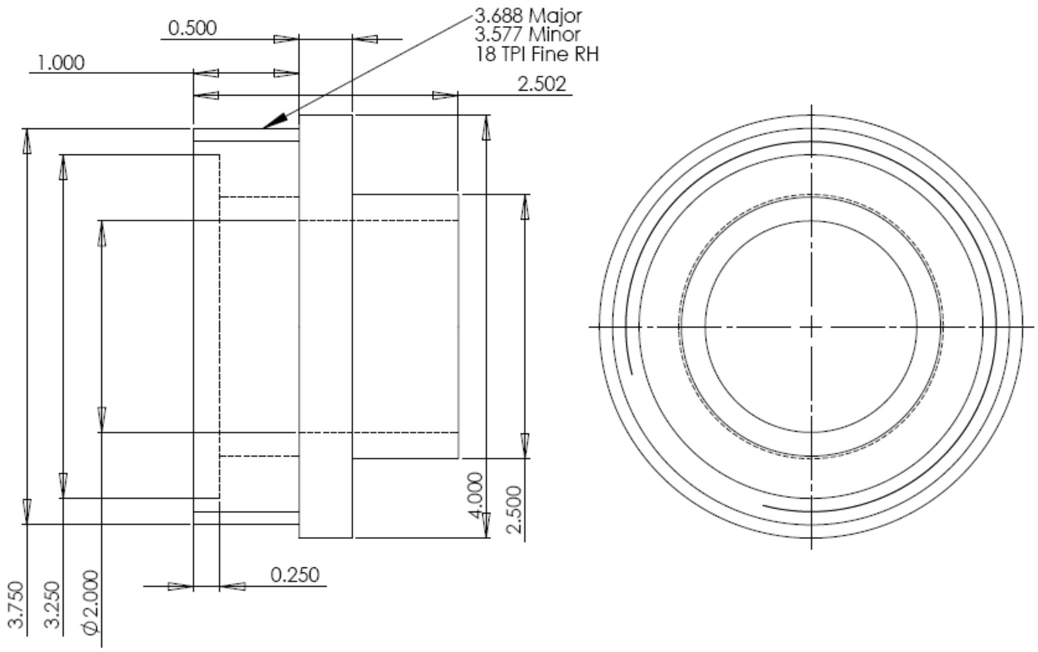

Figure 24: Nozzle End Cap Construction Drawing

Figure 25: Safety Equipment when Machining Graphite
(Note: Tuck All Hanging Cords into Shirt before Machining)

D. Fuel Grains

This hybrid setup utilizes hydroxyl-terminated-polybutadeine, HTPB, as the fuel, a tire rubber and common binder in solid rocket fuels. Alone it is non-combustible, very stable and safe to handle. There are various blends available, we use HTPB R45M obtained from Aerocon Systems[12] with PAPI 94 as a curing agent. Experiments with the fuel grains were conducted by using additives such as: castor oil, carbon black, Silicone oil, dioctyl adipate

[12] Aerocon Systems, http://www.aeroconsystems.com/

(DOA), and dibutyltin dilaurate cure catalyst (DBDTL). The goal of the additives was to reduce bubble formation by decreasing the viscosity of the mixture so bubbles can escape easier, decrease the brittleness of the fuel grain, and reduce the glass transition temperature to prevent cracking of the grain. These additives in particular were chosen based off of recommendations from the Aerocon website, the MaCH-SR1 project reports from the University of Colorado, Boulder (Alagic, et al. 2006), and John Campbell from SpaceDev (now Sierra Nevada Corporation). Castor oil and silicone oil are used to reduce the viscosity of the mix and allow easier blending and escape of bubbles. Dioctyl adipate is used to make the grain softer and more flexible and dibutyltin dilaurate cure catalyst is used to decrease the curing time for the mixture.

Historical testing had made attempts towards vacuuming, but a successful apparatus was never achieved. Mason jars with a composite layup vacuum pump were used to remove the air and bubbles from the grain. This method resulted in lots of bubbles at the top and cured HTPB with solid pieces at the bottom. Due to the bubbles, only the bottom of the grains could be used. Shaping the grains in the mason jar also posed a problem because the center core molding piece could not be accurately secured and too much post-molding processing was required. It was determined that a proper apparatus for vacuuming the grains would be too costly for the current budget as it would need to hold a strong vacuum on a large amount of fuel while still being able to stir and mix it; experimenting with additives and mixture ratios proved sufficient so that funds can be utilized on the overall test setup and oxidizer system.

Initial tests were conducted using previous molds and samples of 50 to 60 grams; the tests are shown in Figure 26. Thirteen molding tests were completed varying mixture ratios and curing techniques to obtain the best fuel consistency; the various experiments are organized in Table 1. The mixtures from Cure Tests 7 and 8 are highlighted in green since they produced the most promising and consistent results. These cures were expected to produce the best performance out of the motor. Cure test 9 is highlighted in red because it cured too rapidly while being poured and was unusable.

Figure 26. Initial 60 gram fuel grain tests.

Table 1. Fuel Grain Mixture Experiments

		HTPB	PAPI 94	Castor Oil	Carbon Black	DOA	Silicone Oil	DBDTL
Test	Total Mass (g)	Ratio	Ratio	Ratio	Ratio	Ratio	Ratio	Ratio
1	63.0	84.13%	9.52%	6.35%	0.00%	0.00%	0.00%	0.00%
2	63.7	83.20%	10.52%	6.28%	0.00%	0.00%	0.00%	0.00%
3	60.5	86.78%	12.23%	0.99%	0.00%	0.00%	0.00%	0.00%
4	61.0	85.08%	12.95%	1.97%	0.00%	0.00%	0.00%	0.00%
5	61.0	85.08%	13.77%	1.15%	0.00%	0.00%	0.00%	0.00%
6	60.8	83.88%	13.16%	2.96%	0.00%	0.00%	0.00%	0.00%
7	60.0	84.00%	12.00%	4.00%	0.00%	0.00%	0.00%	0.00%
8	60.5	83.14%	12.40%	3.97%	0.50%	0.00%	0.00%	0.00%
9	61.0	83.44%	12.13%	3.28%	0.00%	0.82%	0.16%	0.39%
10	60.4	83.28%	12.58%	2.98%	0.00%	1.16%	0.05%	0.05%
11	60.0	83.00%	12.00%	4.00%	0.50%	0.50%	0.05%	0.00%
12	61.0	81.15%	11.97%	3.93%	0.49%	2.46%	0.10%	0.00%
13	200.0	84.00%	12.00%	4.00%	0.00%	0.00%	0.00%	0.00%

Heated tests were conducted placing the molds in a metal cabinet with two halogen lamps to provide the heat during the curing process. The same mixture was used for both hot and cold cure tests, the results are shown in Figure 27. It was found that heating the grain to temperatures around 130 °F as it cured increased the number of bubbles as well as their respective size. From these results we determined that cold cures of the HTPB would be sufficient once the optimal mixture ratio was found.

Figure 27. Cold Cure (left), and Hot Cure (right)

As aforementioned, cure tests 7 and 8 produced the best results showing a large reduction in bubbles with no large pockets present. Figure 28 shows cure 7 and Figure 29 shows Cure 8. Cure 7 used 84% HTPB with 12% PAPI curing agent and 4% castor oil. This produced a very flexible and elastic mold with only tiny bubbles spread evenly throughout. Despite any additional additives, no cure resulted with less bubbles. Carbon black was added to this mixture at a ratio of 0.5% resulting in cure 8. This mold was slightly stiffer than cure 7 due to the carbon addition and it was estimated that the carbon would improve heat transfer during the combustion process (Chiaverini and Kuo 2007).

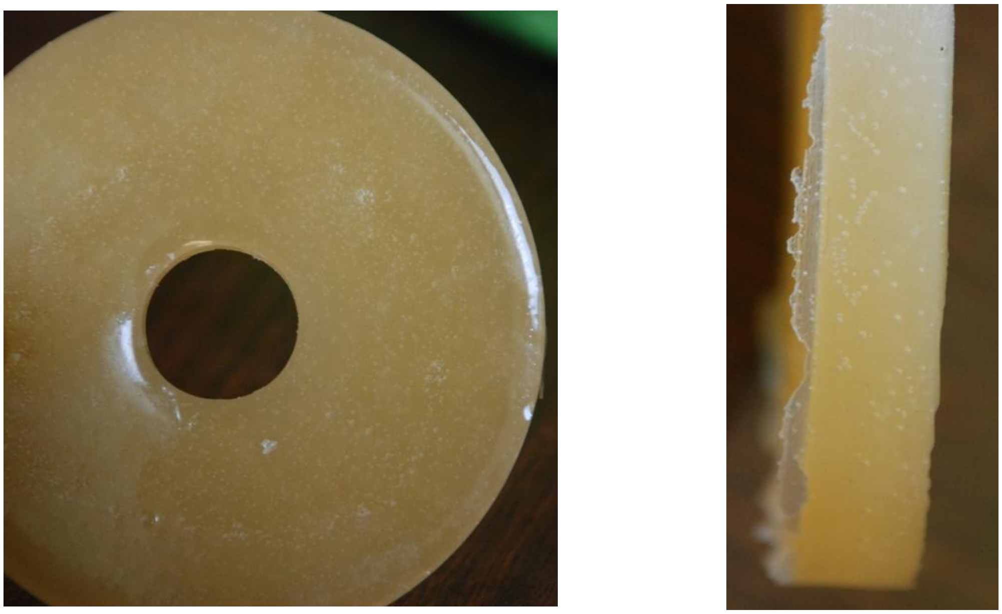

Figure 28. Fuel Cure 7

Figure 29. Fuel Cure 8

A large scale mold test was conducted as cure 13 with this mixture ratio to verify that scaling the mold size would not have major affects to the quality of the grain. Figure 30 shows the results of the cure; the consistency and quantity of bubbles was identical to that seen in the small scale cure.

Figure 30. Cure 13: Large Scale Fuel Cure

1. Fuel Grain Molds

New molds were created to assist in curing the fuel grains for motor test fires. Previously, only one fuel mold was available for curing, greatly increasing the curing time to obtain an entire grain set for a test fire. The new molds, Figure 31 and Figure 32, allow for curing three grains simultaneously. They also have a much simpler compression-fit design, as opposed to a threaded design, increasing simplicity and facilitating removal of the grain after it has cured. They also contain two PVC pipes in the center of the mold to provide the core geometry for the grain. The use of two pipes allows for interchangeability of the outer to adjust the core geometry for various shapes and sizes for experimentation in fuel regression properties.

Figure 31. Fuel Molds

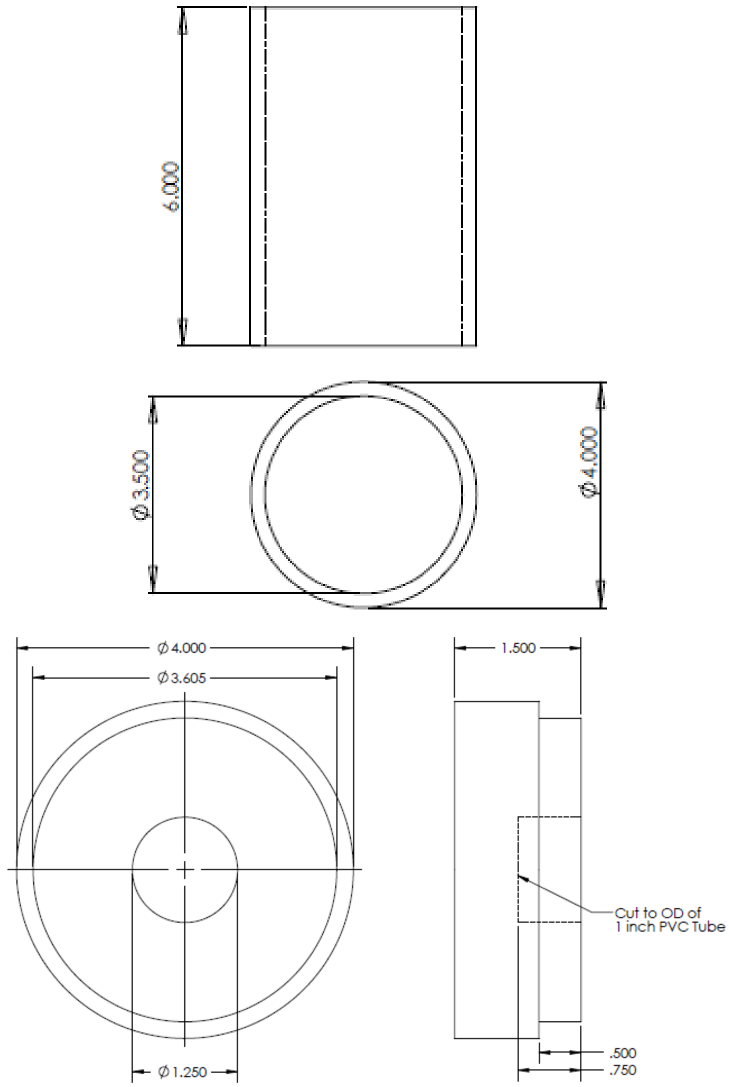

Figure 32. Fuel Mold Dimensions

A film of petroleum jelly is applied to the aluminum mold and PVC pipe core. This lubricant assists in the removal of the grain from the mold after curing. Custom fuel grain liners have also been researched from the Precision Paper Tube Company[13]; using a resin impregnated cardboard (phenolic tube) would be the best option for aiding in grain removal. Grain liners would also be beneficial for fuel grain compression and heat transfer during combustion. Use of these liners is the next step in fuel grain manufacturing once an increased budget is established. The full procedures for curing fuel grains are shown in the appendix.

2. Fuel Curing

Three 525 gram mixes were made to provide a complete set of fuel grains for a test fire. The HTPB, castor oil, and carbon black are first mixed and allowed to sit for one hour before adding the PAPI curing agent. This hour set time allows the HTPB to outgas and help reduce the number of bubbles that result. Figure 33 shows the fuel mixes ready for pouring.

After adding the PAPI curing agent, a mixer attached to a drill was used to ensure a thorough blend throughout the grain, Figure 34.

[13] Precision Paper Tube Company, http://www.pptube.com/

Figure 33. Fuel Mix with Carbon Black

Figure 34. Fuel Mixer

The effort put into the mixing process has a substantial impact on the resulting fuel grain; not enough mixing will prevent the grain from curing. Figure 35 shows the resulting grains once cured.

Figure 35. Cured Fuel Grains

III. Testing Facilities

A. Test Stand

The test stand shown in Figure 36 is used for all hot and cold flow tests done on the motor. For the purposes of this project it was relocated from the hangar test cell to the Aerospace Engineering department propulsion lab (building 41-144) and repaired. It is rated to take thrust loads up to 2500 lb_f and is mounted to the floor via 4 forged eye bolts connected to turnbuckles mounted to ½" bolts into the cement floor. Breakaway boards and wiring were hooked up for valve control and sensors using the existing wiring in the lab, Figure 37 and Figure 38.


Figure 36. Hybrid Test Stand

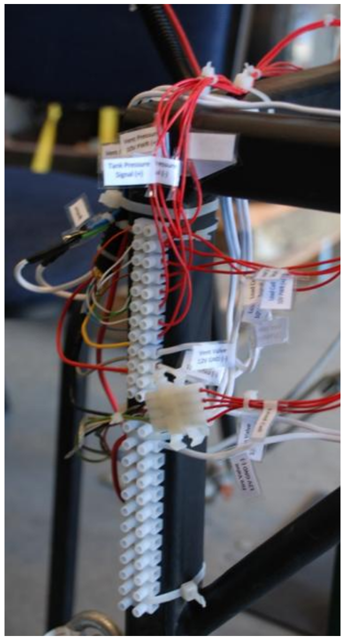
Figure 37. Test Stand Wiring

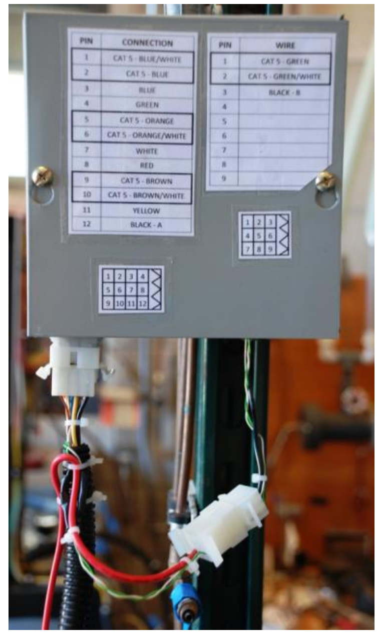

Figure 38. Lab Connections

B. Control Box

A portable control box was also constructed to operate all of the valves and ignite the motor remotely. It operates off a rechargeable 12 volt lead acid battery to provide for lab and field use when the oxidizer tank is filled on the field prior to liftoff. Battery operated control of the valves also allows for the system to be depressurized in the event of a power failure. The box contains two arming circuits, one for filling and one for firing the motor. A buzzer activates when the firing system is armed thereby warning all personnel involved of danger. The box is shown in Figure 39 and a circuit diagram in Figure 41. Opening the solenoid valves requires continuous current, but the fire valve only requires a trigger signal. This is due to the separate control circuit for the valve actuator; a modified H-bridge allows remote control of the valve circuit using a separate power source; sending high currents through the building's sensor wiring is not advisable. The valve control circuit is shown in Figure 40.


Figure 39. Portable Control Box

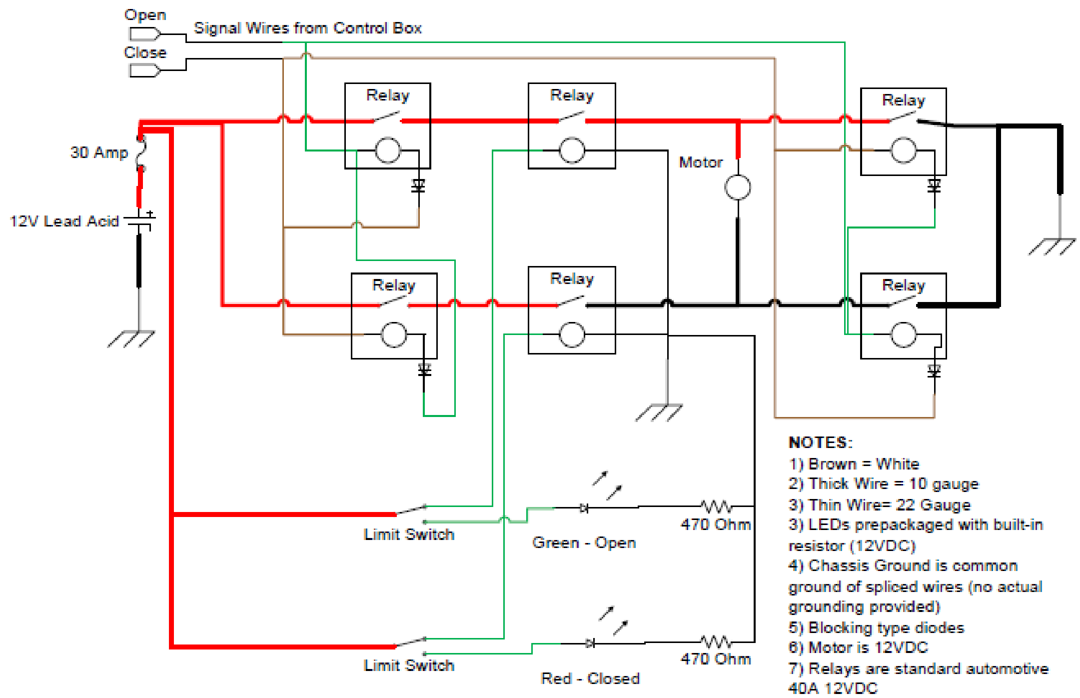

Figure 40. Modified H-Bridge Valve Control Circuit

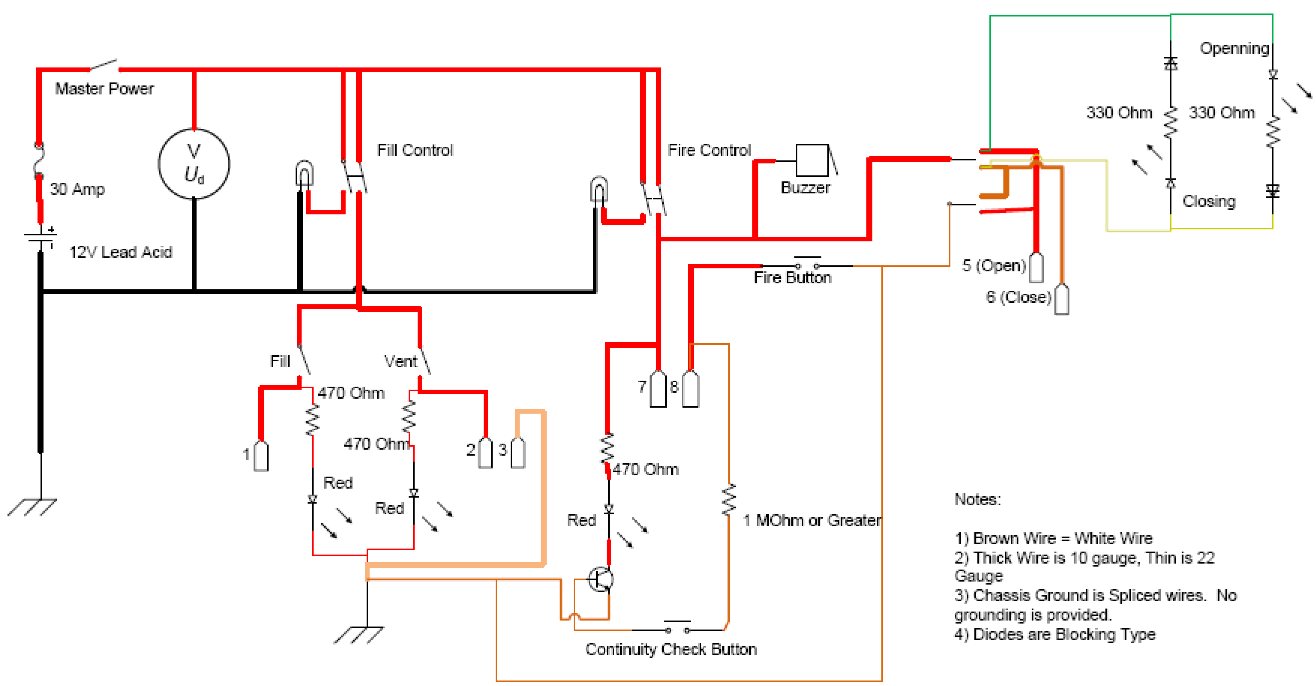

Figure 41: Control Box Circuit Diagram

C. Sensors and LabVIEW Data Acquisition

Two pressure transducers with a 1 to 1000 psi_g range and two load cells are utilized to obtain nitrous oxide pressure, tank weight, and motor thrust. The pressure transducers, Omega model PX302-1KGV, are located on both the fill and vent assemblies; this provides both liquid pressure and gaseous pressure of the nitrous oxide during the filing process. Once the oxidizer tank is filled the fill side is removed and only gas pressure is obtained during the fire. The oxidizer tank hangs from one load cell, an Omega model LCFD-50 with a 1 to 50 lb_f range, to obtain nitrous mass during filling and firing. The other load cell, an Omega LC101-500 with a 1 to 500 lb_f range, is mounted to the top of the stand and measures thrust using a moment arm. The moment arm has an adjustable fulcrum to account for various thrust predictions and ensure accurate data without damaging the sensor. All of the sensor data is routed through a National Instruments USB-6008 DAQ and into LabVIEW. Data is displayed and recorded to a Microsoft Excel spreadsheet for processing. Test data shows that an external low band pass filter may be beneficial and is recommended for future testing.

D. Risks and Risk Mitigation

The Aerospace Engineering Department regularly runs a hybrid rocket experiment for a lab classroom activity at a demonstration-sized thrust level. Due to the propellant and energy levels produced in the CPSS motor, much more care than usual must be taken for safety to ensure all components operate as designed. It also requires a flight oxidizer tank to be filled from a supply tank and then dumped during the test instead of firing directly from the supply tank; this provides additional safety since the flight tank can only hold up to 7 lbs of nitrous oxide in comparison with the supply tank which holds 50 lbs of nitrous. The following table details system and component risk followed by mitigations for each. Note that general test procedures are to be followed every time the motor is operated. Additionally, test procedures tailored specifically to the test being conducted are written up prior to any testing occurring. These procedures must include any amendments to the general rules, procedures, and information specific to the test such as test goals, expected results, and additional potential hazards or risks.

Table 2 shows the risks with this setup and how they are mitigated.

Table 2. Risks and Mitigation

Risk	Mitigation
Nitrous Oxide Inhalation and Suffocation	• Both lab roll-up doors shall be fully open during all testing providing maximum ventilation. • A minimum of 5 minutes shall be allowed after large scale nitrous dumping to allow for fumes to evacuate the test area. • The nitrous oxide doesn't inherently have a smell. It comes with sulfur dioxide additive to enable detection by smell and prevent recreational inhalation. • Only 1 person is allowed in the test area while the tank is pressurized during standard procedures.
Tank or Fitting Rupture or Burst	• Tank rated to 3000 psi with a built-in 3.4 factor of safety, yielding an effective 10.48 factor of safety. • All fittings rated to operate at up to 3000 psi, allowing a 5.0 factor of safety.
Filling Valve Stuck Open	• Manual shutoff valve located before the electronic valve to prevent flow to the flight tank from the supply tank. • Tank supply valve.

Venting Valve Stuck Open	• Adjustable needle valve located between the tank and the electronic valve can be used to prevent continuous escape of flow. • Relatively small amount of nitrous storage capability of 7 pounds in the flight tank, so the main valve can be used to purge the entire system.
Power Outage	• All control circuits and valves run off of batteries, enabling operation in the event of a power outage.
Spontaneous Combustion of Nitrous Oxide	• Non-combustible gas requires dissociation before ignition can occur. • Can decompose at temperatures as low as 550K which is not achievable in the oxidizer system. • Nitrous Oxide can react with bearing, valve seats, and seals made from Teflon and krytox; it can also react with PTFE but only at 630K. These materials have been eliminated from the system or used minimally.
Spontaneous Combustion of HTPB	• HTPB is a very stable and inert rubber commonly found in tires, it has a flash point of > 400 °F in an open container and isn't capable of spontaneous combustion.
Tank Over Pressurization	• Two pressure transducers located on the tank assembly monitoring both gas and liquid pressures. • Addition of 1800 psi burst discs on the tank manifold ensure 3000 psi component ratings are never reached.
Combustion Chamber Over Pressurization	• Combustion chamber design to 1900 psi, enabling 1.9 factor of safety. • Increased combustion chamber pressure above oxidizer tank pressure will increase backpressure on the injector preventing flow to continue effectively choking off the oxidizer and stopping combustion.
Generation of Higher than anticipated Thrust	• Test stand rated to 2500 lb_f of thrust with an expected thrust of 300 lb_f allowing an 8.3 factor of safety.

IV. Non-Steady State Analysis

A. The System and Interrelations

In order to simplify calculations the following overall assumptions were made:

1) Isentropic flow of an ideal gas
2) Adiabatic compression and expansion of gasses
3) Oxidizer and exhaust are perfect gasses
4) Burn temperature is constant enough to assume constant
5) Combustion stops when either fuel or oxidizer run out
6) Oxidizer is self pressurized
7) Single cylindrical core burn grain geometry
8) Gas in chamber can be considered as in a stagnant state

B. Intentions

The intention of this analysis was to obtain thrust curves and approximate total impulses for a NOS/HTPB hybrid rocket motor. The analysis was conducted to apply modularity such that the same concepts expressed here could be used for other rocket projects. As a note of warning, the equations presented here are correct in concept; however a unit check is required before implementation.

1. The Nozzle

Since force and impulse are the required solutions, analysis starts at the nozzle. Force is described as a combination of a jet and hydraulic force shown in Eq. 2 (Sutton and Biblarz 2001). Impulse is the time integral of this force, Eq. 3. Finally specific impulse describes efficiency, Eq. 4.

(2)

(3)

(4)

Since a simple DeLaval converging-diverging nozzle is assumed, the isentropic flow equations can be used. However, a check must be done to ensure choked flow; this is done by finding the Mach number at the entrance to the converging section. Starting with Eq. 5 and the mass flow rate described by Eq. 6, Eq. 7 is used to determine the Mach number.

(5)

(6)

(7)

A_1 is the geometric intake area of the convergent section of the nozzle if and only if there is significant spacing between the nozzle convergence and the end of the grain port. If this is not true, you must assume that the intake area of the nozzle is the exit plane area of the grain port. The theoretical compression area ratio required to choke the flow is obtained from Eq. 8 (Zucrow and Hoffmann 1976).

(8)

Comparing this to the actual compression ratio we find that if ε_{theo} is greater than ε_1 then the nozzle is not choked and therefore it can be considered a smooth orifice where the mass flow rate is defined by Eq. 9 (Huzel and Huang 1992), the exit velocity is defined by Eq. 10, and the exit pressure is defined by Eq. 11.

(9)

(10)

(11)

If ε_{theo} is equal to or within 98% of ε_1, to prevent oscillations in the numerical simulation, then we can consider the nozzle choked. By choking the nozzle, the mass exiting is now restricted by the isentropic flow relationship of Eq. 12 (Zucrow and Hoffmann 1976). The exit velocity is defined by Eq. 13 (Sutton and Biblarz 2001), and the exit pressure is defined by Eq. 14 (Zucrow and Hoffmann 1976).

(12)

(13)

(14)

P_1 is assumed to be equal to P_{ch} since the chamber gasses are considered stagnant; the same goes for T_1. Given that no flow separation occurs, Mach number at the exit plane, M_E, is a geometric constraint and must be back solved using Eq. 15 (Zucrow and Hoffmann 1976).

(15)

2. The Chamber

The Combustion Chamber is characterized as a control volume where all energy entering or leaving the system is in the form of a mass flux. Therefore, the mass of a perfect gas in this control volume is the time integral of Eq. 16.

(16)

As stated by the conservation of mass, if the mass in the combustion chamber increases so does the pressure to compensate and vice versa. The internal pressure, P_{ch}, can therefore be described in a quasi-steady state as the time integral of Eq. 17.

(17)

The internal temperature, T_{ch}, is solved through experimental data. Since HTPB is a polymer and not covered under the JANNAF tables, experimental temperature data from Figure 42 is adjusted for nitrous oxide oxidizer and resolved as Eq. 18. Whereas the data represented below is particular for swirl injected gaseous oxygen the assumption was made that by the time the oxidizer reaches the fuel grain it has already decomposed into its constituents and the oxidizer to fuel ratio can be modified, using molecular weights, to adjust for the extra nitrogen.

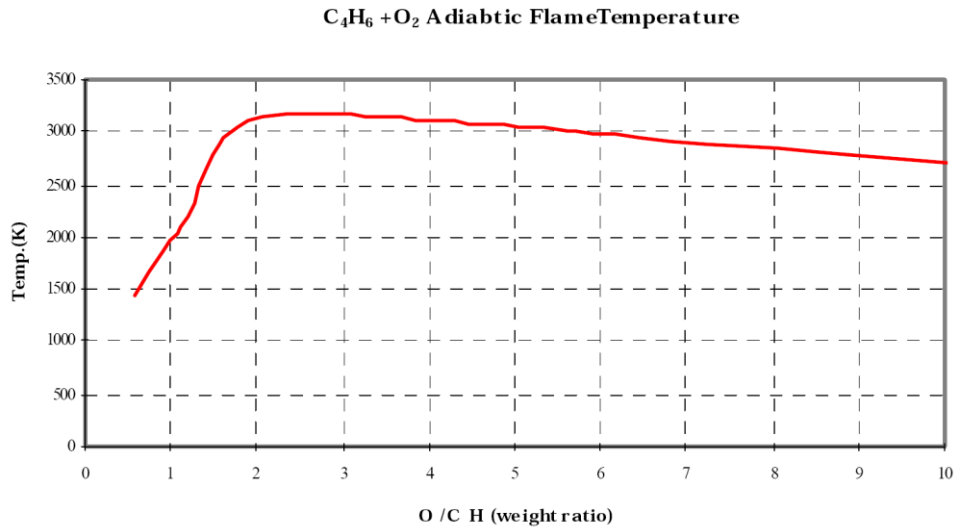

Figure 42: Experimentally Derived HTPB Combustion Temperature (Lee and Potapkin 2002)

(18)

Where

(19)

The gas constant of the combusted gasses was found by applying molar mass of the combustion components to the ideal gas constant, 8.3145 J/(K-mole). The molar mass of nitrous oxide is 44.013 grams/mole and the molar mass for a monomer of HTPB is approximately 54.09 grams/mole. From these values, the exhaust gas constant, R_E, in inch-lb_f / lb_m-°R is described by Eq. 20

(20)

This equation is illustrated in Figure 43; the gas constant of nitrous oxide, R_{Ox}, by itself is 0.1889 J/(g-K) or 265.20 inch-lb_f / lb_m-°R.

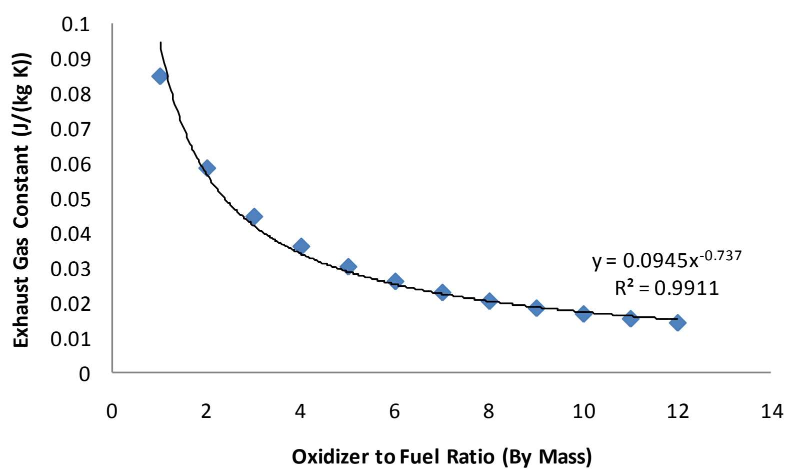

Figure 43: Exhaust Gas Constant

The mass of the gas in the chamber is the time integral of Eq. (16). The chamber volume is the sum of the geometric free space which is described by the grain port. Therefore the initial volume is expressed by Eq. 21.

(21)

This volume, $\cancel{V}_{ch}$, changes with time as defined by Eq. 22.

(22)

Equation 21 and Equation 22 assume a constant radial regression along the entire length. However, as with many other hybrid rockets, one can expect to see more regression near the injector orifice and less towards the nozzle end. There are many models for fuel regression in hybrid rocket motors, yet they are all too specific and not applicable to our case. It was decided to develop a layman method which can characterize any core burning hybrid rocket grain. To begin the grain is split into sequential cylindrical grains each dl in length as in Figure 44.

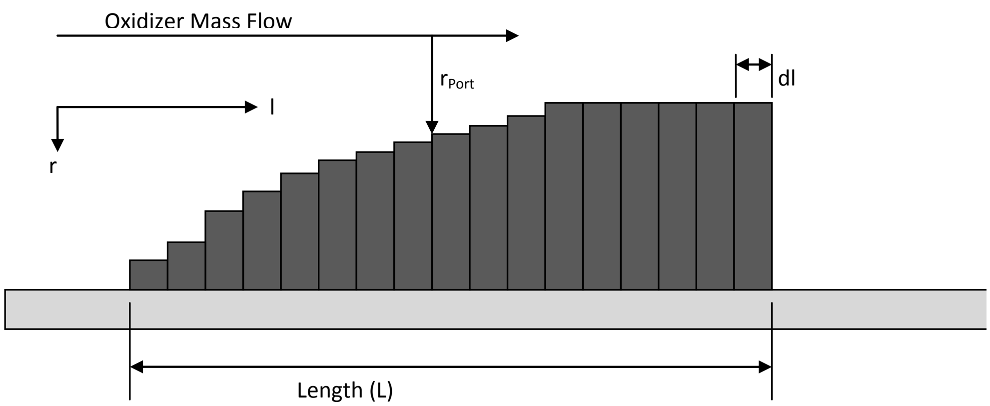

Figure 44: Regression Model Dimensions

Each section is characterized by the fuel regression equation, Eq. 23 (Sutton and Biblarz 2001), by setting a, n, and r_{port} as discrete functions of length; only the oxidizer mass flux at the point of injection is considered. In any case, fuel grain regression is defined by Eq. 23 (Sutton and Biblarz 2001). If a and n are functions of length then it is defined by Eq. 24. In addition, if a_l, n_l and r_{port} are functions of Length, l, then Eq. 25 applies. The regression variables must be experimentally derived for each test case.

(23)

(24)

(25)

3. The Injector

The transient solution for the oxidizer mass flow, is fairly easy to solve as a function of the pressure drop from the oxidizer storage tank and chamber, however all equations require some experimentally derived values. The experimentally derived values for this injector are outlined in Table 3. It was determined that the head loss coefficient did change as a function of mass flow from testing, as shown in Figure 45.

Table 3: Experimental Injector Values

Head Loss Coefficient (K_{inj})	44.25
Diameter of Injectors (d_{inj})	3/32 inch
Number of Injectors (N_{inj})	12
Density of NOS_{Liquid}	51.32 lb_m/ft^3

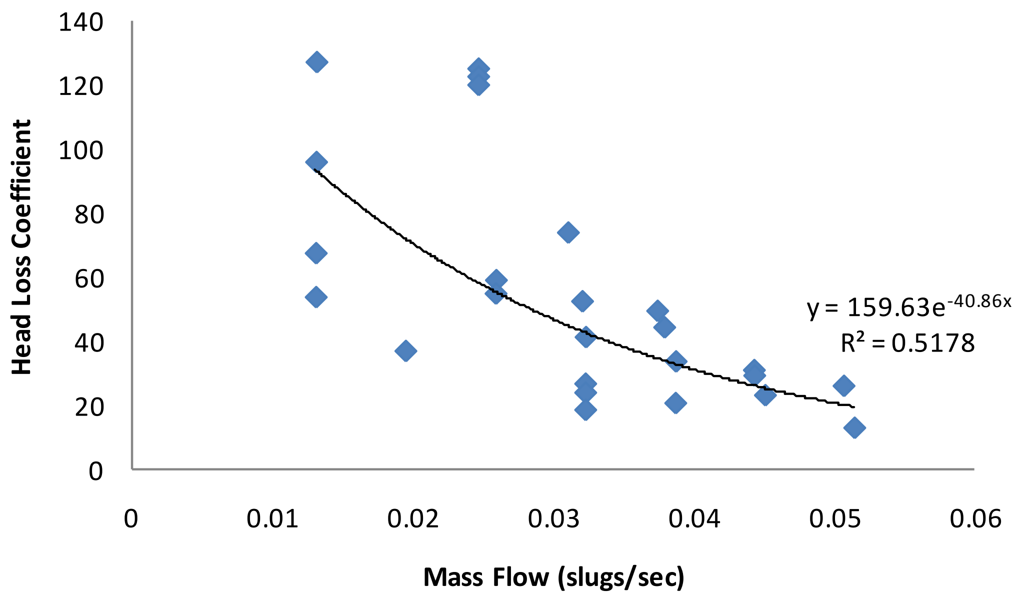

Figure 45: Head Loss Coefficient Related to Mass Flow

The noise in the readings, R^2 = 52%, was deemed too large to apply this phenomenon to the model, however additional testing may prove this application necessary. From this data, mass flow is estimated by Eq. 26 (Huzel and Huang 1992).

$$ - \qquad \frac{\qquad}{\qquad} \qquad (26)$$

This equation applies to any injector as long as the assumption of liquid flow is made. The experimental values in Table 3 were derived from the system operating in full test configuration. Testing the injector at a pressure drop comparable to actual flight will result in a more applicable performance prediction.

4. The Oxidizer Tank

The final variable is tank pressure, P_T. There are two methods to solve for this variable: the adiabatic model, which only applies when the oxidizer is pressurized higher than its vapor pressure at operating temperatures from the beginning to the end of the burn, and the energy method, which applies in our case and any case where the oxidizer self pressurizes the tank on the vapor boundary.

Adiabatic Model

The adiabatic model works the same way as gas moving a piston. Pressurant applies force to the top of the fluid meniscus causing it to move; some mixing, or frothing of the liquid, will occur resulting in a decreased density particularly nearing the end of purge. The pressure can be described by Eq. 27, with the initial condition, C_1, defined by Eq. 28.

(27)

(28)

The pressure in the tank is a function of volume rather than time, therefore oxidizer mass remaining must be tracked as a function of time.

Energy Method

Since the oxidizer in our case is self pressurizing we must use the vapor dome, Figure 46, to resolve its static pressure. The system starts with internal energy, Eq. 31. Assuming that the burn is short, the argument was made that the only energy leaving the system is the enthalpy of the mass flow out of the control volume, , which is called in the following equations. The gas does perform work in the form of accelerating the liquid mass of the oxidizer through the injector; this work is characterized by Eq. 29. Therefore the internal energy, U, of the system can be described as the time integral of Eq. 30 (Moran and Shapiro 2000) where the initial condition is solved in Eq. 31.

(29)

(30)

(31)

(32)

(33)

From Figure 47 and the quality, Eq, 32, the enthalpy of the mixture is described in Eq. 34 (Moran and Shapiro 2000).

(34)

Figure 47 shows a direct correlation between the enthalpy of the mixture and the pressure of the system. Therefore, the tank pressure can be determined by solving the enthalpy equation for pressure, Eq. 35.

(35)

However, enthalpy as described in Eq. 34 and Figure 47 is a function of quality. What this means is that we must know the mass of the liquid and gaseous components at all times. Since nitrous oxide boils there is a mass flux within the control volume which must be account for. Since no model of this phenomenon has been found in research we propose Equation 36. Therefore the liquid mass can be described as Equation 38 and gaseous mass as Equation 38. Coefficient, G_B, is an experimentally derived variable we call the boiling flux. From our experience it should be related to the diameter and/or characteristic length of the tank. From these experiments, G_B, is found to be near 1.3 however further research is required.

(36)

(37)

(38)

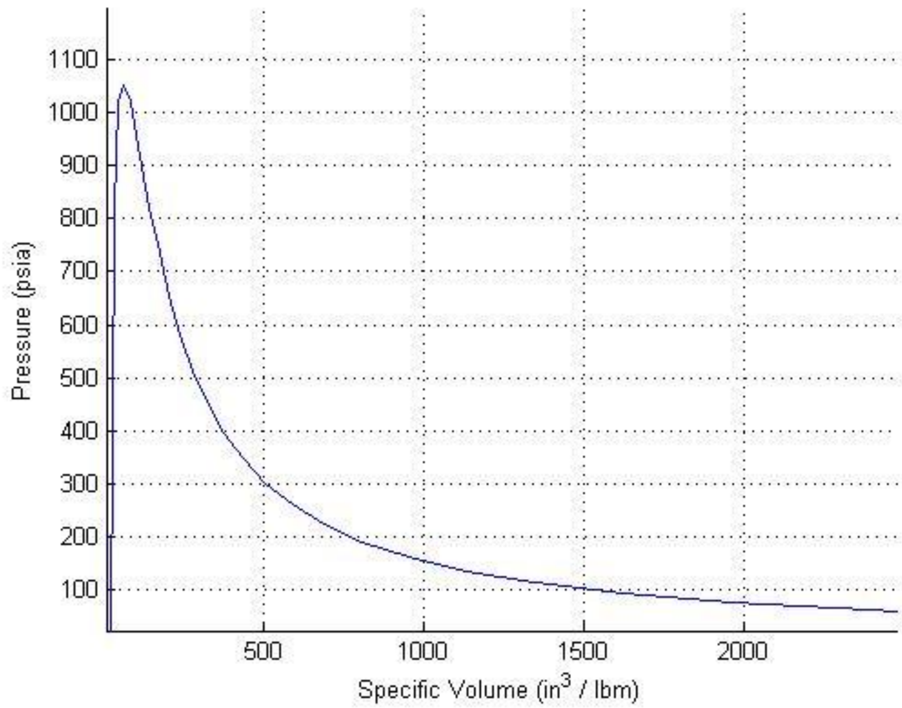

Figure 46: Nitrous Oxide Vapor Dome (ESDU International plc 1991)

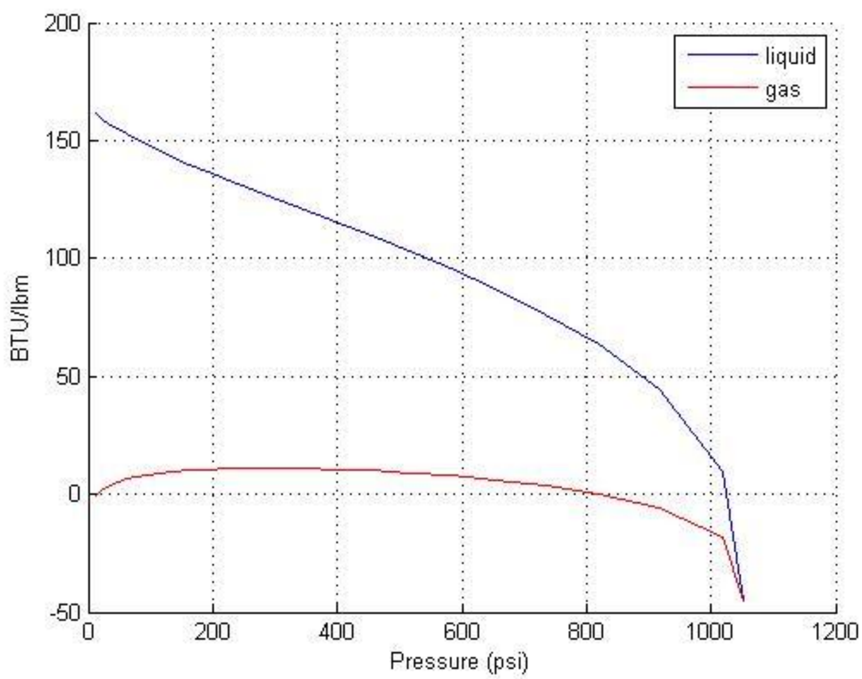

Figure 47: Nitrous Oxide Enthalpy Diagram (ESDU International plc 1991)

V. Results

A. Test Results

1. *Fuel Grains*

The post fire analysis was conducted in two parts, a visual inspection of the rocket motor components and an analysis of the data collected. The visual inspection of the fuel grains showed the most regression occurring at the injector or forward fuel grain. The middle fuel grain showed the second most regression and the aft fuel grain closest to the nozzle showed the least amount of regression. This result was expected due to the design of the injector. The injector was designed to force the oxidizer outward towards the fuel grain to increase mixing between the fuel and oxidizer. The increased mixing and the high velocity of the oxidizer, which aids in the erosion of the fuel grain, both contribute to the increased regression rates. It is believed that a substantial level of entrainment occurred in this forward fuel grain. Entrainment occurs when a liquid layer of fuel develops on the fuel grain surface and a high oxidizer mass flux into that surface creates instabilities, such as with a swirl injector. These instabilities expel atomized liquid fuel from the fuel surface into the combustion zone. Expulsion of atomized liquid fuel from the surface as opposed to gasified fuel is believed to greatly reduce the blowing factor (resistance to heat transfer) and increase performance (Chiaverini and Kuo 2007).

The forward fuel grain also showed spiral grooves carved by the oxidizer as shown in Figure 48. The groves in the fuel grain were at a constant 30 degrees from the horizontal which was also predicted due to the angle of impingement of the injector ports. Since the injection port diameters are equal, the flow velocity from each hole is equal and the vector sum of the angles yields a 30 degree spiral. This spiral groove starts at the forward end of the grain and ends mid way into the second fuel grain. The spiral grooves show the erosion of the fuel grain caused by the oxidizer which proves that the injector causes a spiral within the combustion chamber as designed. The spiral grooves dissipate half way into the second grain which suggests that the spiral force of the oxidizer yields to the combustion forces within the motor at this location. It is suspected that the boundary layer characteristics of hybrid combustion (blowing factor, heat transfer, and pyrolysis) dominate at this point. However, during test fires gasified fuel can still be seen swirling while exiting the nozzle once the oxidizer tank runs out of liquid oxidizer for combustion. This opposes typical hybrid regression characteristics in which higher regression is seen towards the aft end of the motor due to increased mixing and more complete combustion along the length of the motor.

Figure 48: Cut away view of the forward fuel grain showing 30 degree spiral grooves.

2. *Injector*

After the test fire, a visual inspection of the injector was also conducted. The injector showed some damage at the center cone. The purpose of the center cone is to aid in the expansion of the oxidizer causing it to phase change from a liquid to a gas and to guide the oxidizer outwards towards the fuel grains. By forcing the oxidizer outwards towards the fuel grains, a recirculation zone was created at the center of the combustion chamber. From post test observations it was determined that this recirculation zone caused hot gasses to move forward towards the injector and melt the cone section. During the first test fire the cone end of the injector was made of aluminum held by a stainless steel screw and completely melted away. For the second test fire, a steel cone held by a zinc coated steel screw was used which also melted, but not as significantly as the aluminum cone used at the first test fire; however it welded with the screw. Figure 49 shows the injector face with the cone section melted away from both test fires.

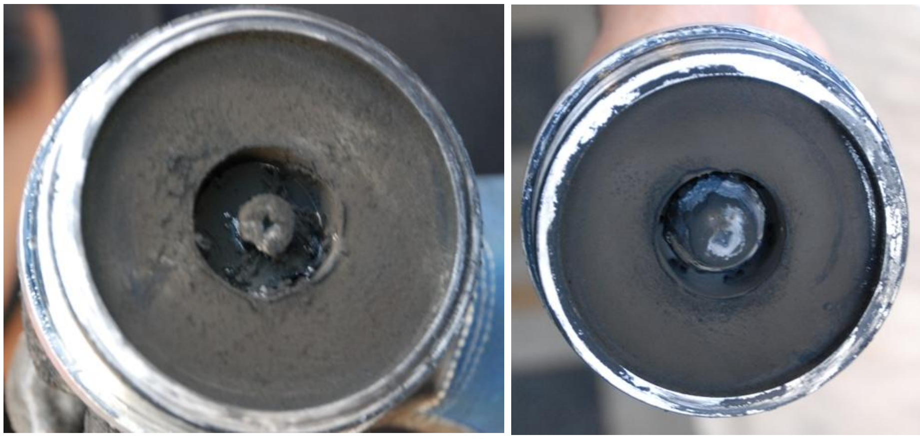

Figure 49: Injector damage due to a recirculation zone in the center of the combustion chamber which melted away the cone section of the injector.

3. Test Fire Performance

Before hot fire tests were conducted, a fill test along with a cold flow test of the injector manifold was conducted. The purpose of the fill test was to verify the amount of liquid nitrous oxide that the supply tank can fill the flight tank. From the fill and vent system the supply tank was able to fill the flight tank to approximately 6 pounds of nitrous oxide. Also, the fill system was able to pressurize the flight tank to within 10 psi of the supply tank bringing the pressure of the flight tank to approximately 600 psi.

The results of the cold flow test through the injector shows that at 600 psi in the flight tank and a release into atmospheric pressure, the mass flow of oxidizer through the injector is approximately 1.3 lb_m/sec. **Error! Reference source not found.** and **Error! Reference source not found.** shows the flow pattern of the nitrous exiting the injector during the cold flow test. It can be visually seen and confirmed in **Error! Reference source not found.** and **Error! Reference source not found.**, by the apparent swirl lines, that the nitrous oxide leaving the injector is being swirled. This verifies the CFD model and initial flow pattern expectations of the injector.

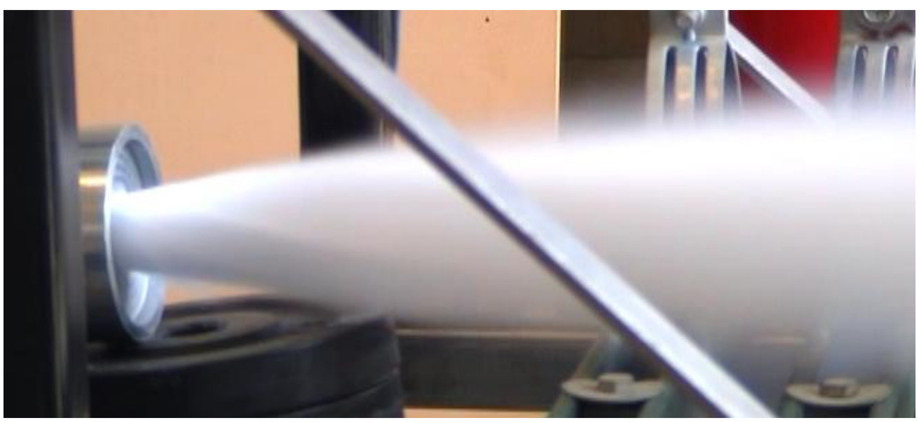

Figure 50: Nitrous Oxide Injector Cold Flow Test View 1

Figure 51: Nitrous Oxide Cold Flow Test View 2

The first test of the HM4 rocket motor was conducted on May 11, 2010 and resulted in a combustion chamber over-pressurization. This over-pressurization occurred 0.2 seconds after ignition due to a premature release of the NOX. Analysis and evaluation of the combustion chamber failure showed that release of the nitrous oxide must be delayed until the APCP ignition grain has completely burned. The over-pressurization occurred as the high pressure nitrous oxide came into contact with the combusting APCP grain; this high pressure contact resulted in an atomization of the APCP grain and a violent flash of extremely high speed combustion. This failure analysis was verified when small pieces of unburned APCP ignition grain were found in the test area, and with further ignition testing. A still image from the test video is shown in **Error! Reference source not found.**.

From the ignition testing it was determined that a smaller amount of APCP is sufficient to start the motor, and the size of the APCP ignition grain has no significant impact on the regression rate or mass flux of the fuel. The only impact of the APCP grain size is on the wait time between ignition and release of the nitrous oxide. Previously, 50 grams of 54mm APCP grain was used to ignite the motor; following the ignition testing the APCP grain was reduced to approximately 10 grams.

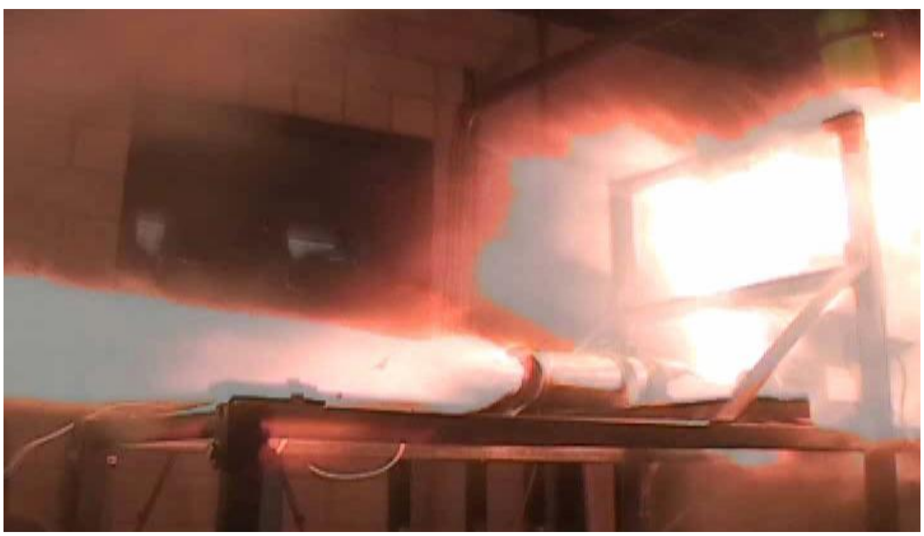

Figure 52: Combustion Chamber Over Pressurization

Error! Reference source not found. shows the damage as a result of the over-pressurization. The chamber failed at the forward end by the injection manifold where the ignition grain was located. Fortunately, only a few pieces of hardware were damaged including the single use graphite nozzle, the combustion chamber, and the base piece of the two piece injection manifold. It was decided to reconstruct the combustion chamber at a shorter length to fit three 4.5 inch long fuel grains. The base piece of the injection manifold was also increased in length to provide better structural support of the thrust load for testing.

Figure 53: Combustion Chamber Damage

The first successful test of the motor conducted on May 25, 2010 resulted in 247 lb_f of peak thrust, 212 lb_f of average thrust for 6 seconds; the test is shown in **Error! Reference source not found.**. This yielded a specific impulse of 160 seconds and a total impulse of 1,400 lb_f-seconds (6228 N-s), placing HM4 in the low M-class for amateur rocket motors. Much of the data obtained from this test was used to validate and compare with our computer model. An oxidizer mass flux of 1.13 lb_m per second was obtained with a total oxidizer mass of 6.8 lb_m at an average of 500 psi_g. The fuel regressed at a mean rate of 2.92 mm per second. This high regression rate resulted in a fuel mass flux of 0.189 lb_m per second.

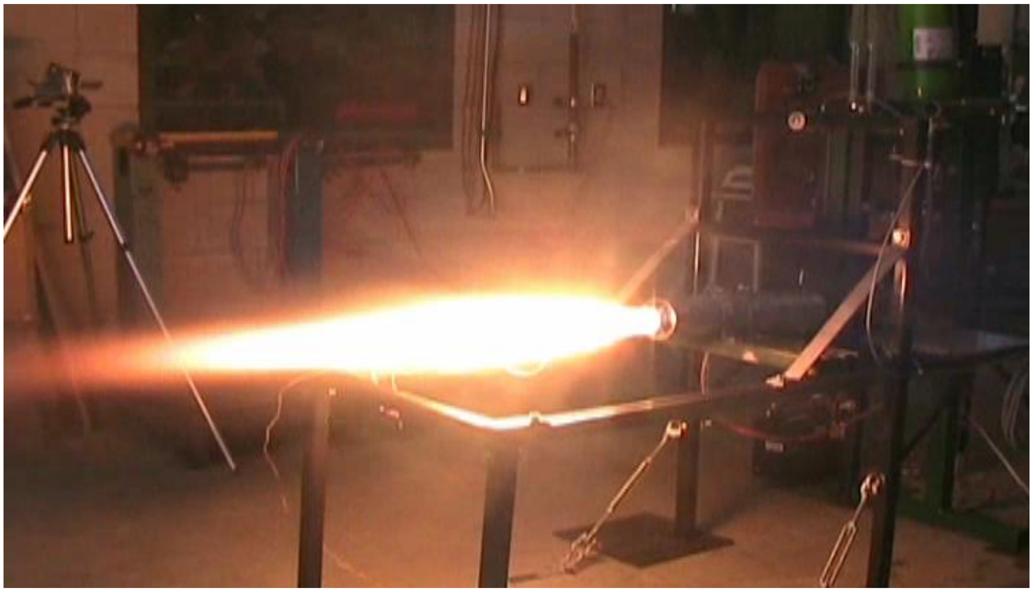

Figure 54: Successful Test Fire

The second successful test was conducted on June 1, 2010 and resulted in a peak thrust of 338 lb_f and an average thrust of 260 lb_f for 6 seconds. This test yielded a specific impulse of 200 seconds and a total impulse of 1,623 lb_f-seconds (7,260 N-s). This test duplicated the same test conditions as the first and obtained nearly identical results; the only differences were due to the changes in tank conditions. A tank mass of 7 lb_m of nitrous oxide was obtained at an initial 588 psi_g. An oxidizer mass flux of 1.104 lb_m per second and a fuel mass flux of 0.170 lb_m per second were obtained yielding an average mixture ratio of 6.5. **Error! Reference source not found.** summarizes all of the test results in English units and **Error! Reference source not found.** summarizes the data in SI units.

Table 4. Summary of Test Results in English Units

Test	Peak Thrust (lbf)	Average Thrust (lbf)	Burn Time (seconds)	Total Impulse (lbf-sec)	Specific Impulse (sec)	Regression Rate (in/sec)	Oxidizer Mass Flux (lbm/sec)	Fuel Mass Flux (lbm/sec)	O/F Ratio
1	247	212	6	1,400	160	0.1153	1.130	0.189	5.98
2	338	260	6	1,623	200	0.0880	1.104	0.170	6.49

Table 5. Summary of Test Results in SI Units

Test	Peak Thrust (N)	Average Thrust (N)	Burn Time (sec)	Total Impulse (N-sec)	Specific Impulse (sec)	Regression Rate (mm/sec)	Oxidizer Mass Flux (g/sec)	Fuel Mass Flux (g/sec)	O/F Ratio
1	1,099	943	6	6,228	160	2.929	512.6	85.7	5.98
2	1,503	1,157	6	7,219	200	2.235	500.8	77.1	6.49

B. Analysis

1. Regression Analysis

Initial estimates for the regression rate of around 1 to 1.5 mm per second were taken from classical hybrid models located in Chiaverini[14]pending empirical data from testing. Once two tests were conducted and empirical regression rates were found to be in excess of 2 mm per second our own regression rate was derived. Utilizing the basic regression model in Eq. (39) and the observed regression rates from the two test fires, our own empirical constants, or a and n values, were determined to generate a regression prediction based on the oxidizer mass flux, G_{ox}. From our data we obtained a value of 0.027909 and an n value of 11.607 to get Eq. (40).

(39)

(40)

Other regression models were considered for use in our analysis but didn't match well with our test setup. It was found that each regression model is derived specifically for each test setup to determine the relationships between the various parameters being tested; these parameters include injection method, fuel and oxidizer combination, and combustion process. Our test setup is very unique due to its custom 12 port self-impinging swirl injector and fuel composition. Further analysis into higher fidelity and complex regression models to accurately predict the regression rate as a function of length down the combustion chamber would benefit further experimentation in injection methods.

2. Performance Analysis

The rocket's performance after each test fire is calculated using equations from Sutton[15]. Since the transient data in regards to tank mass is ridiculously noisy the average mass flow of oxidizer and fuel are used to calculate average oxidizer to fuel ratio and I_{sp}. Specific results are tabulated in **Error! Reference source not found.**.

From the MATLAB model, the overall thrust curve results are shown in Figure 55. This transient thrust prediction almost matches the experimental results from the first successful test fire. The model showed an average oxidizer mass flow of just under 1.1 lb_m/sec and an average regression rate of 0.085 inch/sec which matches closely with averaged test results of 1.117 lb_m/sec and 0.102 inch/sec respectively. The tank pressure during testing and the

[14] (Chiaverini and Kuo 2007)
[15] (Sutton and Biblarz 2001)

simulation dropped from the initial pressure of 590 psi_g to around 400 psi_g over the course of 6 seconds. This proves the validity of the energy method described in the analysis section, Section IV. Further experimentation to solve the new empirical constant is necessary however. Tank blow-down tests conducted with nitrous oxide dumping through a flight injector into a chamber of fixed pressure and various volumes are recommended.

The quick drop in thrust which occurs in the simulation at around 5 seconds can be explained through the assumption of saturated gas and saturated liquid. The drop occurs when the liquid oxidizer runs out. The lower density mass flow of gaseous oxidizer reduces fuel burn and overall thrust. The test results show that at this time the motor is still generating thrust. The only explainable solution is frothing. It is believed that the mixture in the tank is not a perfectly separated gas and liquid mix. While pockets of both in the saturated state may exist, the overall mixture is a foamy mix similar to soap bubbles not in the idealized model of a gas pushing a solid piston. Therefore the average mass flow after this point is different and cannot be predicted with our current solution.

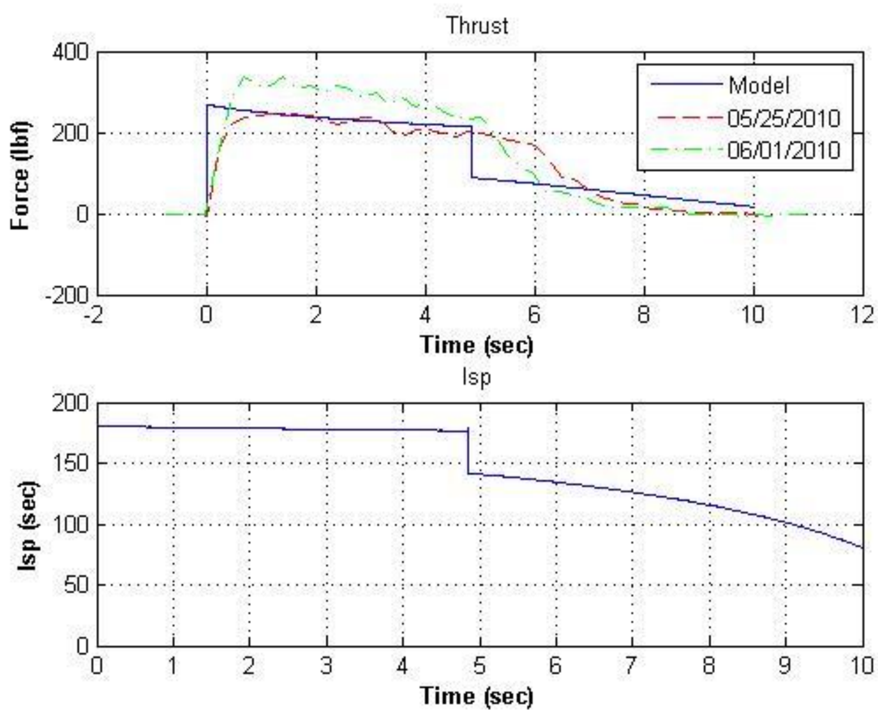

Figure 55: Comparison of Model Results to Test Fire

VI. Conclusion

As a continuation of the hybrid rocket motor project undertaken by the Cal Poly Space Systems club the revitalization of project hardware, establishment of facilities for testing, and production of additional hardware to greatly increase performance and safety was accomplished. Previous iterations of the design had developed a fair baseline and level of experience regarding experimental performance and testing methods. From that foundation the two prime goals of increased oxidizer mass flow and consistent fuel curing were accomplished. Emphasis put towards safety was and continues to be of utmost importance. Development of a complete list of procedures including those for off nominal performance was paramount prior to any tests occurring; this ensured the safety of all parties involved. Every component designed and built has met or exceeded safety requirements. These efforts towards safety as well as a compiled list of the associated risks and how they are mitigated has enabled a faultless safety record. Emphasis towards accurate and easily understood documentation has also been made to enable future development and experimentation to occur smoothly and unhindered.

The revisit to the oxidizer feed and injection system has allowed for a complete redesign and reconstruction with safety rated components. Drag in flow passages and insertion losses through controls were reduced drastically by reducing the number of fittings and components from the tank to the injector. In addition, atomization and mixing of the oxidizer was improved using a self-impinging swirl injection method. Fuel composition and consistency have also reached a new level. Uniformity and consistency of the cure were increased in addition to reducing bubble formation. Fuel mixture research and process development have been established to expedite the fuel curing process and facilitate future fuel research. Finally, a transient computer model has been developed to predict future test fires and to optimize the motor. Despite all these tremendous efforts to establish this foundation there is still work to be completed. Continued hot fire testing will provide insight into the yet fully understood phenomena occurring and establish a much more accurate transient model of the nitrous oxide tank and fuel grain regression; these models will enable more accurate performance predictions.

This project taught the benefits of experimentation. Most of the solutions sought did not have clear answers. Trouble was often encountered in finding simple conceptual answers to questions and instead high fidelity over-specific analysis had to be developed. Initial experiments were all accomplished using everyday materials to qualitatively solve issues particularly those of injector flow pattern and cure consistency. Every increase in fidelity and quality of experiment provided substantial additional information used to design and build the current iteration of the motor; however, without the smaller and much simpler experiments to give guidance early efforts made towards the final design would have been misguided. In contrast, the use of heritage hardware and documentation provided much frustration due to its lack of accuracy. Care must be taken to ensure all conclusions are rooted in scientific fact and found with sound reasoning. When doubt comes to mind one must not underestimate the value of simple basic experiments and calculations from the engineering fundamentals to provide guidance. Validation and verification of all decisions and designs ensures optimum results.

Our hopes are that this project sees further research. Much more testing can and should be done to further investigate and model what is occurring. Some specific areas for future study and experimentation include varying fuel grain geometries, fuel additives, injection swirl angles, number of injection ports, and nozzle geometries and types. As always, funding puts limitations on the amount and quality of work that gets done; one must always be economical in purchases and consider items of greatest utility. Manufacturing is a lengthy and time consuming process, so schedules, commitment, and responsibility become vital.

In summary, documentation and definitive results in predicting performance of a hybrid rocket motor were attained without injury or loss of property while passing on the engineering knowledge learned through experience to the next generation of engineers.

Appendix

I. Method for Machining Angled Holes on Injector

i. Angle the mill head to the requisite angle
ii. Put in the Tool
iii. Use the top of the center cone as the reference point (Use a CAD program to find the required X and Y travel to locate the holes)
iv. Use Drill Press lever on Mill to perform function
v. Tool Order

1. 1/8 inch flat end mill: Cut only what is required to make a flat surface.
2. #3 Center Drill (May need to be a few inches long to clear part): Drill until the flare hits the part
3. 3/32 Drill Bit or the required size: Drill until you feel no more material removal.

II. Test Procedures

Test Procedures (Revised June 5, 2010)

Safety Features:

Safe Propellants:

The hybrid propellants are non-explosive materials that are non-corrosive and relatively safe under standard conditions of pressure and temperature. HTPB is a rubber that is very safe and easy to store. Nitrous Oxide Plus requires careful handling because of its pressurized storage but is no more dangerous than any other compressed gas.

Secure Ignition:

Hybrid motors will not combust unless there is sufficient heat available to melt the HTPB and break oxygen from the NOX. This means that if there was an oxidizer flow failure and Nitrous Oxide was released into the combustion chamber prematurely there would be **NO COMBUSTION**. Without the heat and pressure from the ignition system there would be no chemical reaction between the HTPB and the Nitrous Oxide. With our redundant safety locks controlling the ignition system we can safely handle the hybrid motor without fear of spontaneous combustion.

Pressure Relief Valves:

The addition of 1800 psi pressure relief pop-off valves on the oxidizer feed assembly located at the tank manifold prevent the system from reaching the yield pressure of 3000 psi. Expected maximum pressure is 800 psi while all fittings and components are rated at 3000 psi, the 1800 psi relief valves ensure the yield pressure is never reached.

Safety Factors:

Oxidizer tank safety factor: 10.48
(1850 psi design / maximum of 600 psi expected) * (3.4 built in safety factor)

Solenoid safety factor: 3.67
(2200 psi design / maximum of 600 psi expected)

Ball Valve safety factor: 5
(3000 psi design / maximum of 600 psi expected)

Hosing safety factor: 5
(3000 psi design / maximum of 600 psi expected)

Fittings safety factor: 5
(3000 psi design / maximum of 600 psi expected)

Hybrid Motor Test Firing Procedure

Modified from those used during HM1 testing in 2004-2005

Safety Regulations:

1. Everyone **MUST** have eye protection such as safety glasses. Prescription glasses are **NOT** sufficient. Those without eye protection must stand 100 ft away during pretest procedures and may not under any circumstances operate any part of the apparatus. People with eye protection still must be as far back as possible during pre-testing and a minimum number of people may be involved in operating the apparatus.
NOTE: Ear protection is available but not required.
2. Prior to pre-testing setup there must be a **first aid kit**, a **fire extinguisher** (Class B or multi-class including B), a **water hose**, and a **phone** for calling emergency response (land line is preferred). All participants must be aware of the location of these items and knowledgeable in how to use them.
3. For the firing **NO ONE** may view the motor by direct line of sight. Control room safety windows and video cameras will be used to monitor and document the motor.
4. A heavy-duty physical barrier (i.e. wall) must be between the motor and any persons within 500 ft of the firing.
5. If there are any violation of these rules or if anyone places themselves in any position that could potentially be harmful, testing will be suspended immediately.
6. Absent an advisor, the President is the final authority on any sequential firing attempts.
7. Level of authority for test firing in order of highest to lowest is Faculty Advisor, President, Vice President, and Propulsion Lead. The firing may not commence without the physical presence of either the Advisor or President. The Vice President may fill the role of the President only if the President gives express permission. Additional oversight may be required and will take precedent over the order above.
8. Written procedures specifically tailored to the test must be created and approved by the President **prior** to testing. These procedures must include any amendments to the general rules and procedures and information specific to the test such as test goals, expected results, and additional potential hazards or risks.

Hybrid Motor Test Fire Procedures:

1. <u>Roles during Test Fire</u>
   1.1. **Test Control (Propulsion Lead):** Command and control during firing.
   1.2. **Fire Control:** Operates all filling, venting, and firing valves as well as the ignition circuit. Will shut off all control circuits in the event of an Abort.
   1.3. **Safety Control:** Will be the only person to approach any fire with an appropriate fire extinguisher after being instructed to do so by Test Control.
   1.4. **Range Safety (multiple):** Stands watch at predetermined positions to prevent bystanders from approaching the test area. Will have radio communication to Test Control.
   1.5. **Sensor Control:** In charge of all sensors and data acquisition during the test.

2. <u>Sensor Calibration</u>

2.1. Pressure Transducers **NOTE: Pressure transducers only need be checked to ensure their calibration is still accurate; they do not need to be calibrated each test fire.** 2.1.1. Open the "CPSS Hybrid Program" LabVIEW file and power the sensors to 10 V DC. 2.1.2. Obtain a reference voltage for atmospheric pressure. 2.1.3. Connect a compressed air line to the pressure transducer through its valve assembly. 2.1.4. Increase pressure on the compressor in increments of 5 or 10 psi, record each voltage output by the transducer. 2.1.5. Apply a linear fit and input the slope and y-intercept into the LabVIEW block diagram to obtain psi gauge pressure readings. 2.1.6. Repeat for the 2^{nd} pressure transducer.
2.2. Load Cells **NOTE: Load cells need to be calibrated for each test fire to ensure accuracy.** 2.2.1. Ensure no load is applied to the load cell and record reference voltage. 2.2.2. Apply weights to the load cell using rope in increments of 5 to 10 pounds, record each voltage output by load cell. 2.2.3. Apply a linear fit and input the slope and y-intercept into the LabVIEW block diagram to obtain lb_f load readings. 2.2.4. Repeat for the 2^{nd} load cell.

3. Fuel and Combustion Chamber Preparation

3.1. Take photos of the combustion chamber, injector, and nozzle for post fire comparison.

3.2. Measure and document all fuel mixture ratios and dimensions being used.

3.3. Cut a counterbore into the top of one of the fuel grains to fit the 10g, 54mm APCP ignition grain.

3.4. *Nozzle*

3.4.1. Put a film of white lithium grease in the base section of the aluminum nozzle end cap and insert the graphite nozzle.

3.4.2. Put a bead of RTV adhesive around the lip of the converging portion of the graphite nozzle.

3.4.3. Put a thin film of white lithium grease around the remaining exposed base of the aluminum nozzle end cap and place the graphite converging section snug against the aluminum nozzle end cap.

NOTE: Do NOT allow RTV adhesive to contact between the graphite and the aluminum. It will PERMANENTLY bond them together.

3.4.4. Ensure the RTV adhesive fills all the gaps between the graphite pieces and wipe away any excess.

3.4.5. Lubricate an O-ring with lithium grease and place it over the forward end of the graphite converging section.

3.4.6. Screw the aluminum nozzle end cap into the combustion chamber.

3.5. *Ignition Source*

3.5.1. Carefully slice a 10g section of 54mm APCP (ammonium perchlorate) solid motor fuel grain.

3.5.2. Carefully slice into the inner diameter of the APCP to place a black powder pellet.

3.5.3. Wedge an E-match (electronic match) in the center of the black powder pellet and AP solid motor fuel grain, cross the wires so there is no chance of static charge buildup.

NOTE: The ignition source is now dangerous and must be treated with extreme care.

3.6. *Fuel Grains*

3.6.1. Grease the inside of the combustion chamber and the outside of each fuel grain with a film of white lithium grease.

3.6.2. Insert the aft fuel grain all the way into the chamber until it rests against the convergent section of the graphite nozzle.

3.6.3. Place a thin film of RTV adhesive between each fuel grain, sliding each all the way into the chamber one at a time; insert the ignition APCP at the top of the middle fuel grain.

3.6.4. Lubricate the motor side threads of the injection manifold and an O-ring with white lithium grease.

3.6.5. Place the greased O-ring on the top of the first fuel grain, and then attach the injection manifold to the combustion chamber.

NOTE: Ensure there is slight fuel grain compression when sealing the nozzle and injection manifold to the combustion chamber.

4. <u>Oxidizer System Preparation</u>

4.1. Attach the brass hex tank manifold to the flight tank using a Teflon washer.

NOTE: NEVER use Teflon tape for connecting the tank manifold to the flight tank.

4.2. Roll up **BOTH** lab doors.

4.3. All hose and fittings (NPT Threads) must be sealed with Teflon tape but not allow exposure of the Teflon to the flow. Leave the first 1-3 threads exposed to ensure compliance.

NOTE: NEVER use Teflon tape for CGA connections or other straight threads.

4.4. Supply Assembly

4.4.1. Wheel the NOX and GN_2 (gaseous Nitrogen) supply tanks into lab and securely strap them to the pole.

4.4.2. Verify that the blue manual valve on fill hose is **CLOSED**.

4.4.3. Connect the regulator to the GN_2 supply tank.

4.4.4. Connect the fill hose to the GN_2 regulator.

4.5. Vent Assembly

4.5.1. Verify the vent solenoid circuitry, test operation, and ensure it is **CLOSED**.

NOTE: Solenoid circuit gets VERY HOT during use. Minimize continuously powering the solenoid to avoid overheating.

4.5.2. Connect the pressure transducer to the T-fitting.

4.5.3. Connect the needle valve to vent solenoid.

NOTE: Needle valve should be fully OPEN.

4.5.4. Connect the vent assembly to the brass hex tank manifold at the quick disconnect.

4.5.5. Connect the pressure transducer to the vent pressure wiring channel.

4.5.6. Connect the solenoid to the vent valve wiring channel

4.6. Feed Assembly

4.6.1. Connect the steel braided feed hose to the brass hex tank manifold.

4.6.2. Connect the fire valve motor to power and the control circuit.

4.6.3. Power the fire valve circuit, check for audible actuation of 2 control relays and illumination of its indicator lights.

NOTE: GREEN indicates the valve is open, and RED indicates closed.

4.6.4. Test the fire valve actuation by cycling it open and closed.

NOTE: Visually inspect that the ball valve and the micro switches for wear.

4.6.5. Connect the free end of the steel braided feed hose to the fire valve, ensuring the fire valve is **CLOSED**.

4.6.6. Connect the ½” hex brass pipe to the fire valve on the motor side.

4.6.7. Connect the tank load cell to the load cell wiring channel and record the empty weight reading.

4.7. Fill Assembly

4.7.1. Verify the fill solenoid circuitry, test operation, and ensure it is **CLOSED**.
4.7.2. Connect the pressure transducer to the T-fitting.
4.7.3. Connect the fill hose to the fill assembly.
4.7.4. Connect the fill assembly to the brass hex tank manifold at the quick disconnect.
4.7.5. Connect the pressure transducer to the tank pressure wiring channel.
4.7.6. Connect the solenoid to the fill valve wiring channel.

5. <u>Nitrogen Flush</u>

5.1. **OPEN** the GN_2 supply tank valve.
5.2. **OPEN** the GN_2 regulator to 150 psig.
5.3. **OPEN** the blue manual valve on the fill hose.
NOTE: Ensure that the needle valve on the vent assembly is still fully OPEN.
5.4. Remove all personnel from the test area **AND** shut the control room doors.
5.5. **ARM** the Fill System and **OPEN** the fill solenoid from the control room until the tank reaches 150 psig.
5.6. **OPEN** the vent solenoid for 5 seconds.
NOTE: This cleans out the vent system
5.7. **DISARM** the fill system.
5.8. **CLOSE** the GN_2 supply tank valve.
5.9. Remove all personnel from the test area **AND** shut the control room doors.
5.10. **ARM** the fire system and **OPEN** the fire Valve until the system completely depressurizes.
NOTE: This cleans out the oxidizer feed system.
5.11. **DISARM** the fire system and **CLOSE** the GN_2 regulator and blue manual valve on the fill hose.
5.12. Disconnect the fill hose from the GN_2 regulator.

6. <u>Secure to Test Stand</u>

6.1. Apply Teflon tape to the hex brass ½ inch NPT pipe from the fire valve.
6.2. Slide the combustion chamber into the test stand mounts and tightly secure itto the test stand.

7. Fill Procedure

7.1. Check NOX Flow

7.1.1. Connect the fill hose to the NOX supply tank
7.1.2. **OPEN** the NOX supply tank valve.
7.1.3. Check for leaks.
NOTE: Propulsion Lead must decide whether any leaks are acceptable before firing. The Advisor and President have the power to overrule the Propulsion Lead's decision. Unacceptable leaks are those which result in visible white exhaust or bubbling of evaporating oxidizer. An example of an acceptable leak would be one in which the exhaust is clear.
7.1.4. **OPEN** the blue manual valve on the fill hose.
7.1.5. Check for leaks.
7.1.6. Remove all personnel from the test area **AND** shut the control room doors.
7.1.7. **ARM** the fill system and **OPEN** the fill and vent solenoid from control room until 100 psig in the tank is reached.
7.1.8. **DISARM** the fill system and check for leaks.
NOTE: Leaks may occur due to shrinkage of fittings from the extreme cold of NOX.
7.1.9. Remove all personnel from the test area **AND** shut the control room doors.

7.2. Flight Tank Filling

7.2.1. **ARM** the fill system and **OPEN** the fill and vent solenoid from control room until a steady state pressure is reached (near 600 psig). Watch the fluid exiting the vent assembly and listen for audible changes in fluid flow.
NOTE: Filling process takes several minutes. Watch the pressure levels and vented fluid carefully. Cycle the valves open and closed and check for leaks as necessary.
7.2.2. **DISARM** the fill system and check for leaks due to fitting shrinkage.
7.2.3. **CLOSE** the NOX supply tank valve.
7.2.4. Disconnect the fill assembly from the brass hex tank manifold at the quick disconnect.
NOTE: Be VERY CAREFUL when disconnecting the fill assembly; it is very difficult to disconnect and a small burst if nitrous oxide will be released as the quick disconnects shut. Wearing gloves and a full face shield is recommended.
7.2.5. Record the full weight reading from tank load cell.

7.3. Fill Hose Purge

7.3.1. Connect the fill assembly quick disconnect to the purge connector.
7.3.2. Secure the purge connector to ensure it sprays outside.
7.3.3. Remove all personnel from the test area **AND** shut the control room doors.
7.3.4. **ARM** the fill system and **OPEN** the fill solenoid until the fill hose is empty.
7.3.5. **DISARM** the fill system and **CLOSE** the blue manual valve.
7.3.6. Disconnect the fill hose and wheel the tanks outside the test area and secure for the test fire.

8. Firing Procedure

8.1. Fire Preparation

NOTE: Read Section 8.3 PRIOR to ANY test fire preparation.

8.1.1. Connect thrust load cell to the tank pressure wiring channel.

NOTE: Check that the thrust reading is zero to ensure accurate data acquisition.

8.1.2. Confirm the firing circuit is **DISARMED**.

8.1.3. Short the 2 alligator clips by touching them together ensuring no residual voltage differential lies across them.

8.1.4. Connect igniter leads to ignition alligator clips.

NOTE: Take special care to avoid the exhaust area behind the motor.

8.1.5. **START** the video documentation.

8.1.6. Remove all personnel from the test area **AND** shut the control room doors.

8.2. Safety Check

8.2.1. Confirm that test area is clear of people and debris.

8.2.2. Test Control confirms with Sensor, Fire, and Safety Control with a **GO/NO GO** for test.

NOTE: Sensor control checks all pressure readings for nominal values and Fire Control checks all valves to ensure they are in the correct position.

8.2.3. Test Control confirms with each Range Safety that all bystanders are clear of the test area with a **GO/NO GO** for test.

8.2.4. Test Control declares via radio "Any radio traffic by personnel other then the Test Control will be interpreted as an abort command from this point on."

8.3. Test Fire

8.3.1. Fire Control **ARMS** the firing circuit.

8.3.2. Sensor Control **STARTS** the LabVIEW data acquisition.

8.3.3. Test Control begins audible countdown from 10 seconds.

8.3.4. Countdown transmitted on radio until 5 seconds then clear radio for any abort command.

8.3.5. At 0 Test Control declares "**IGNITION**" and Fire Control ignites the motor.

8.3.6. Wait until the flames from the APCP ignition die down and are almost out, then Test Control declares "**NITROUS ON**" and Fire Control **OPENS** the fire valve.

8.3.7. Visually confirm the valve opens with the **GREEN** indicator light and that the motor starts.

NOTE: If motor DOES NOT start, Test Control declares "ABORT" See Section 11.

9. Shutdown

9.1. After the flight tank empties, the Test Control declares "**SHUTDOWN**".

9.2. Fire Control **DISARMS** all circuits.

9.3. Sensor Control **STOPS** the LabVIEW data acquisition.

9.4. Test Control or Safety Control **STOPS** the video documentation.

10. Post Firing Inspection

10.1. All personnel wait at least 5 minutes before entering the test area following inspection by Safety Control or Test Control.

10.2. *Nitrogen Purge*

10.2.1. Wheel the GN_2 supply tank into the lab and secure it to the pole.

10.2.2. Disconnect the motor from the fire valve.
NOTE: Be careful because the motor casing will be VERY HOT.

10.2.3. Attach the fill hose to the GN_2 regulator.

10.2.4. Connect the fill assembly to the brass hex tank manifold at the quick disconnect.

10.2.5. Allow the motor to cool before attempting to remove the injector, nozzle, or fuel grains.

10.2.6. Follow the GN_2 flush procedures in Section 5.

10.3. Component Inspection

10.3.1. Inspect the combustion chamber, nozzle, oxidizer feed assembly, and fire valve for damage.

10.3.2. Remove fuel grains for performance evaluation, weighing, and dimension measurements.

10.3.3. Remove the injection manifold and inspect for damage.

10.3.4. Document all components with pictures for pre-test comparison.

10.4. Clean the oxidizer system component threads with distilled water and simple green and tape over all connections to ensure no contaminants enter.

10.5. Clean the motor and injector with Simple Green and paper towels.

11. Abort

11.1. If motor does not ignite or any abnormalities occur, the Test Control will declare "**ABORT**".

11.2. Any abort will be declared audibly and via radio.

11.3. Fire Control will immediately **DISARM** all circuits.

11.4. All personnel will stay at their stations until Test Control declares the test area safe.

11.5. Safety Control is the only exception and may be instructed to extinguish a fire by the Test Control.

III. MATLAB Codes (Miscellaneous Functions Provided Upon Request to the Authors)

a. Injector Model (Huzel and Huang 1992)

```
% Alexander Athougies
% CPSS
%
% Calculates Nox mass flow through an injector
%
% INPUTS:
% 1) Ninj = number of injectors
% 2) dinj = injector diameter (in)
% 3) Kinj = head loss coefficient
% 4) Psource = source pressure (psia)
% 5) Pdump = pressure of dump point (psia)
% 6) rho = liquid density (lbm/in^3)
%
% OUT:
% 1) dm = mass flow (lbm/sec)

function dm = Injector(Ninj, dinj, Kinj, Psource, Pdump, rho)

rho = rho * (12^3); % lbm / ft^3

if Psource < Pdump
    dm = -(Ninj*pi/4*dinj^2)*(2.238*Kinj/rho/(Pdump - Psource))^(-1/2);
else
    dm = (Ninj*pi/4*dinj^2)*(2.238*Kinj/rho/(Psource - Pdump))^(-1/2);
end

end
```

b. Nozzle Model [(Sutton and Biblarz 2001) and (Zucrow and Hoffmann 1976)]

```
% Alexander Athougies
% CPSS
%
% Calculates Nozzle Thrust and Isp given Dimensions and Mass Flow
%
% INPUTS:
% 1) dm = mass flow expected(lbm/sec)
% 2) P0 = chamber pressure (psia)
% 3) T0 = chamber temperature (R)
% 4) At = throat area (in^2)
% 5) Ae = exit Area (in^2)
% 6) Aet = intake Area (in^2)
% 7) Patm = Atmospheric Pressure (psia)
% 8) Re = gas constant (in-lbf/lbm-R)
% 9) gamma = ratio of specific heats
%
% OUT:
% 1) F = force (lbf)
% 2) Isp = specific impulse (sec)
% 3) dme = real mass flow (lbm/sec)

function [F, Isp,dme] = nozzlecalc(dm, P0, T0, At, Ae, Aet, Patm, Re,
gamma)
```

```
Knoz = 50;
dme = 0;
a = 12*sqrt(gamma*Re*T0/12*32.2);
rho = sqrt(P0/Re/T0);
dt = 2*sqrt(At/pi());

% Find M1
M1 = dm/(a*rho*Aet);

% Find Theoretical Compression Ratio
E1 = 1 / M1*((2/(gamma+1))*(1+(gamma-1)/2*M1^2))^((gamma + 1) / 2 / (gamma
- 1));  % 4.29 - Zucrow

% Find Real E
E = Aet / At;
E2r = Ae / At;

% check choking
if (E1*0.90) <= E
    dme =
At*P0/sqrt(gamma*Re*T0)*(gamma*sqrt((2/(gamma+1))^((gamma+1)/(gamma-1))));
% 4.38 to 4.39 Zucrow
    Me = 1;
    E2 = 0;
    while E2 < E2r
       E2 = 1 / Me*((2/(gamma+1))*(1+(gamma-1)/2*Me^2))^((gamma + 1) / 2 /
(gamma - 1));  % 4.29 - Zucrow
       Me = Me + .001;
    end
    ve = Me*a; % in / sec
    Pe = P0*(1+(gamma - 1)/2*Me^2)^(-gamma / (gamma - 1)); % 4.26 Zucrow
%      while Pe < Patm
%          Pe = P0*(1+(gamma - 1)/2*Me^2)^(-gamma / (gamma - 1)); % 4.26
Zucrow
%          Me = Me - .001;
%      end
elseif E1 > E
    % no choked
    dme = Injector(1, dt, Knoz, P0, Patm, rho);
    ve = dme/At/rho;
    Me = ve / a;
    Pe = P0*(1+(gamma - 1)/2*Me^2)^(-gamma / (gamma - 1));
end

% Find Thrust
if dm > 0 && dme > 0
F = dme*ve/32.2/12 + (Pe - Patm)*Ae; % lbf
Isp = F / dme; % sec
else
    F = 0;
    Isp = 0;
    dme = Injector(1, dt, 1, P0, Patm, rho);
end
```

```
end
```

c. Hybrid Rocket Simulator

```
% Alexander Athougies
% CPSS Hybrid Rocket
%
% Simulator (Rev. 8)...
%
% Assumptions: Isentropic, Adiabatic, Perfect Gas, Incompressible,
% Constant Burn Temps, Combustions stops with fuel/ox (aka. no problems)
%
% function [t,Pt,Pc,rin,mox,mf,F,I,type,avgF] = HybridSim()
function HybridSimRev8()

%% Housekeeping
clc
close all
clear all

%% Inputs
% % CPSS Hybrid
% Simulation
tburn = 10; % sec - simulation time

% Inital Conditions
mox = 6.8; % lbm - Initial Oxidizer Mass - In Tank
Vt = 295 + 24*pi/4*(.5^2); %in^3 - Tank Internal Volume + Line
x = .05; % Quality of Mixture ( % vapor )

% Grain Geometry
L = 13.465; % in - Grain Length
rout = 3.49/2; % in - Outer Radius of Grain
rinp = 1.8/2; % in - Inner Radius of Grain

% Nozzle Geometry
rt = .7/2; % in - Radius of Nozzle Throat
Vfree = 0; % in^3 - free space inside combustion chamber
E2 = 5; % Nozzle Area Expansion Ratio

% Atmospheric Conditions
Pc = 14.7; %psia - Initial Chamber Pressure
Patm = Pc; %psia - Atmospheric Pressure
Tatm = 505; % atmospheric Temp (R)
g0 = 32.2; % ft/sec^2 - Gravity

% Grain Burn Characteristics
a = .28; % Regression Variables - See Excel File
n = .3;

% Injector Geometry
dinj = 3/32; % in - diameter of injector(s)
N = 12; % number of injectors
Kinj = 44.25; % Injector Head Loss Coefficient
```

```
% Chemical Properties
Dome = load('vapordome_nox_v2.mat');
% % Loaded From File
% All Nitrous Vapor Dome Data under structure 'Dome'
g1 = Dome.g1; % Nitrous gamma
g2 = 1.2; % Exhaust gamma
Rnos = 378.5862; % in-lbf / lbm-R (.1889 J / g-K)
% Rex = function of O/F
rhoNOSl = table(Dome.Temperature_E, Dome.density_E_l, Tatm); % Density of
Liquid Nitrous Oxide (lbm/in^3)
rhoNOSg = table(Dome.Temperature_E, Dome.density_E_g, Tatm); % Density of
Gas Nitrous Oxide (lbm/in^3)
rhoHTPB = .0325; % lbm / in^3 - http://www.braeunig.us/space/propel.htm
rhoAIR = 4.34E-5; % lbm / in^3 - Density of Air at T = 20 degC
Pt = table(Dome.Temperature_E, Dome.Pressure_E, Tatm); % Tank Pressure
(psia)

Dome.Af = 1.3; % Boiling Flux Factor

%% Givens
% Nozzle Properties
Aet = pi*rout^2;
At = pi*rt^2;
Ae = At * E2;

%% Calculate Initial Conditions
Vox = (1 - x) * mox / rhoNOSl; % Oxidizer Volume (in^3)
Vf = (rout^2 - rinp^2)*pi*L; % Fuel Mass Volume (in^3)
mf = Vf * rhoHTPB; % lbm
Vu = Vt - Vox; % Initial Ullage Volume (in^3)
mair = (pi*L*rinp^2 + Vfree) * rhoAIR; % Mass of Air in Chamber (lbm)
moxg = x * mox; % lbm
moxl = (1-x) * mox; % lbm
ChamberTemp = Tatm; % R
Ptc = Pt; % Psia
dmoxg = 0;

%% Initial Internal Energy
hg = table(Dome.Temperature_E, Dome.enthalpy_E_g, Tatm); % BTU / lbm
hl = table(Dome.Temperature_E, Dome.enthalpy_E_l, Tatm); % BTU / lbm
ug = hg - Pt / rhoNOSg * 32.2 * 32.2 / 12 / 25037; % BTU / lbm
ul = hl - Pt / rhoNOSl * 32.2 * 32.2 / 12 / 25037; % BTU / lbm
Ut = moxg * ug + moxl * ul; % BTU

% %% In Progress Display
% figure('Name','Display','NumberTitle','off')
% hold on
% display = plot(0,Pt,'rx','MarkerSize',10);
% display2 = plot(0,Pc,'bx','MarkerSize',10);
% legend('Tank','Chamber')
% grid on
% axis([0 tburn 0 800])

%% Main Loop
```

```
% ODETIME = [0,tburn];
ODETIME = linspace(0,tburn,10000);
ODEINPUTS = [Ut, Pc, rinp, moxl, moxg, mf, mair];
ODEOPTIONS = odeset('RelTol',1E-3,'Events',@event);
[t,y] = ode45(@odefcn,ODETIME,ODEINPUTS,ODEOPTIONS);

%% Convert Outputs
Ut = real(y(:,1));
Pc = real(y(:,2));
rin = real(y(:,3));
moxl = real(y(:,4));
moxg = real(y(:,5));
mf = real(y(:,6));
mch = real(y(:,7));

%% Misc Calculations
F = zeros(size(t));
Isp = zeros(size(t));
dmox = zeros(size(t));
dmf = zeros(size(t));
T = zeros(size(t));
Ptc = zeros(size(t));

Ptc(1) = Pt;
rhoNOSl = table(Dome.Temperature_E, Dome.density_E_l, Tatm); % Density of
Liquid Nitrous Oxide (lbm/in^3)
rhoNOSg = table(Dome.Temperature_E, Dome.density_E_g, Tatm); % Density of
Gas Nitrous Oxide (lbm/in^3)

for i = 1:length(t)

    Voxc = moxl(i)/ rhoNOSl;

    % OxMass Flows
    Ttc = Ptc(i)*(Vt - Voxc)/(Pt*(Vt-Vox)/Tatm);
    moxc = moxl(i) + moxg(i);
    if moxc <= moxg(i)
        dmox(i) = Injector(N, dinj, Kinj, Ptc(i), Pc(i), rhoNOSg);
    else
        dmox(i) = Injector(N, dinj, Kinj, Ptc(i), Pc(i), rhoNOSl);
    end

    % Port Radius
    if rin(i) < rout
        Ap = pi * rin(i)^2;
        if dmox(i) > 0
            Gox = dmox(i) / 32.2 / Ap; % slugs/in^2-sec
            rp = a*Gox^n; % in/sec
        else
            rp = 0;
        end
    else
        rp = 0;
    end
```

```
    % Fuel Mass Flow
    dmf(i) = (2*pi*L * rin(i) * rp) * (rhoHTPB); % By rp

    OF = dmox(i) / dmf(i);

    if dmf(i) > 0
        T(i) = GetTemp(OF);
        ChamberTemp = T(i);
    elseif dmf(i) <= 0 && dmox(i) > 0
        T(i) = Ttc;
    else
        T(i) = ChamberTemp;
    end

    % Calculate Force / Isp Outside Loop
    [F(i), Isp(i), dmn] = nozzlecalc(dmf(i) + dmox(i), Pc(i), T(i), At,
Ae, Aet, Patm, Rex, g2);

    % Calculate next Tank Pressure step
    if i < length(t)
        if moxl(i) > 0
            Vl = moxl(i) / rhoNOSl;
            Vu = Vt - Vl;
            rhoNOSg = moxg(i) / Vu; %lbm/in^3
            rhoNOSl = table(Dome.density_E_g, Dome.density_E_l, rhoNOSg);
% lbm / in^3
            hg = table(Dome.density_E_g, Dome.enthalpy_E_g, rhoNOSg); %
BTU/lbm
            hl = table(Dome.density_E_g, Dome.enthalpy_E_l, rhoNOSg); %
BTU/lbm
            H = moxg(i)*hg + moxl(i)*hl;
            Ptc(i+1) = (H - Ut(i)) / Vt * (25037*12/32.2/32.2);
        else
            rhoNOSg = moxg(i) / Vt;
            hg = table(Dome.density_E_g, Dome.enthalpy_E_g, rhoNOSg); %
BTU/lbm
            H = moxg(i) * hg;
            Ptc(i+1) = (H - Ut(i)) / Vt * (25037*12/32.2/32.2);
        end
    else
        Ptc(i) = Ptc(i-1);
    end

    progressbar(i / length(t),'Calculate Thrust')
end

%% PLOTS
figure('Name','Pressures')
hold on
plot(t, Ptc,'--')
xlabel('Time (sec)','FontSize',10,'FontWeight','bold')
title('Tank and Chamber Pressures','FontSize',12,'FontWeight','bold')
grid on
plot(t,Pc,'r')
ylabel('Pressure (psia)','FontSize',10,'FontWeight','bold')
legend('Tank','Chamber')
```

```
figure('Name','Grain Geometry')
plot(t,rin)
title('Port Radius','FontSize',12,'FontWeight','bold')
xlabel('Time (sec)','FontSize',10,'FontWeight','bold')
ylabel('Radius (in)','FontSize',10,'FontWeight','bold')
hline(rout,'r','Max Radius')
grid on

figure('Name','Masses')
hold on
grid on
plot(t, moxl)
plot(t, moxg,'r--')
plot(t, mf,'g-.')
legend('Ox Liquid','Ox Gas','Fuel')
xlabel('Time (sec)','FontSize',10,'FontWeight','bold')
ylabel('Mass (lbm)','FontSize',10,'FontWeight','bold')

figure('Name','Thrust')
subplot(2,1,1)
plot(t,F)
hold on
title('Thrust')
xlabel('Time (sec)','FontSize',10,'FontWeight','bold')
ylabel('Force (lbf)','FontSize',10,'FontWeight','bold')
grid on
plot(Dome.T1(:,1)-.235,Dome.T1(:,2),'r--')
plot(Dome.T2(:,1)-.235,Dome.T2(:,2),'g-.')
legend('Model','05/25/2010','06/01/2010')

subplot(2,1,2)
plot(t,Isp)
title('Isp')
xlabel('Time (sec)','FontSize',10,'FontWeight','bold')
ylabel('Isp (sec)','FontSize',10,'FontWeight','bold')
grid on

save('output.mat')

%% Embedded Fcns
    function dy = odefcn(t,y)
        %         global Ptc
        dy = zeros(7,1);

        %% Get Current #'s
        Utc = y(1);
        Pcc = y(2);
        rinc = y(3);
        moxl = y(4);
        moxg = y(5);
        mfc = y(6);
        mcc = y(7);
        Voxc = moxl / rhoNOSl;
        moxc = moxl + moxg;
```

```
        %% OxMass Flows
        Ttc = Ptc*(Vt - Voxc)/(Pt*(Vt-Vox)/Tatm);
        if moxl <= 0
            dmox = Injector(N, dinj, Kinj, Ptc, Pcc, rhoNOSg);
        else
            dmox = Injector(N, dinj, Kinj, Ptc, Pcc, rhoNOSl);
        end

        %% Port Radius
        Ap = pi * rinc^2;
        if rinc < rout
            if dmox > 0
                Gox = dmox / 32.2 / Ap; % slugs/in^2-sec
                rp = a*Gox^n; % in/sec
            else
                rp = 0;
            end
        else
            rp = 0;
        end
        dy(3) = rp;

        %% Fuel Mass Flow
        dmf = (2*pi*L * rinc * rp) * (rhoHTPB); % By rp
        dy(6) = -dmf;

        %% Get Combustion Temp
        OF = dmox / dmf;

        %          disp(mat2str(OF))
        if dmf > 0
            T = GetTemp(OF);
            ChamberTemp = T;
        elseif dmf <= 0 && dmox > 0
            T = Ttc;
        else
            T = ChamberTemp;
        end

        %% Nozzle Mass Flow
        if dmf == 0
            Rex = Rnos;
        else
            Rex = ExitR(OF); % in-lbf/lbm-R
        end
        [F, I, dmn] = nozzlecalc(dmf + dmox, Pcc, T, At, Ae, Aet, Patm,
Rex, g2); % [lbf, sec, lbm/sec]

        %% Mass of Gas in Chamber
        if moxc <=0
            dmt = -dmn;
        elseif rinc >= rout && moxc > 0
            dmt = dmox - dmn;
        else
```

```
            dmt = dmox + dmf - dmn;
        end
        dy(7) = dmt;

        %% Chamber Pressure
        if moxc <= 0
            Vch = pi*L*rinc^2; % in^3
            Rair = 53.3533*12; % in-lbf / lbm-R
            dPcc = (Rair) * T / Vch * (-dmn); % psia/sec
        elseif rinc >= rout && moxc > 0
            Vch = pi*L*rinc^2;
            dPcc = (Rnos) * T / Vch * dmt;
        else
            Vc = pi*L*rinc^2 + Vfree;
            dVc = (2*pi*L * rinc * rp);
            dPcc = Rex*T *(dmt*Vc - mcc*dVc) / (Vc^2);
%             dPcc = Rex*T*(dmt/Vc + mcc*dVc/(Vc^2));
        end
        dy(2) = dPcc;

        %% Tank Pressure
        if Ptc <= Patm
            Ptc = Patm;
            dUt = 0;
            dmoxg = 0;
            dmoxl = 0;
        elseif moxl > 0
            dmoxg = Dome.Af * dmox / rhoNOSl / (rhoNOSg/(rhoNOSg^2) -
rhoNOSl/(rhoNOSl^2));
            dmoxl = -1*(dmoxg + dmox); % lbm/sec
            Vl = moxl / rhoNOSl;
            Vu = Vt - Vl;
            rhoNOSg = moxg / Vu; %lbm/in^3
            rhoNOSl = table(Dome.density_E_g, Dome.density_E_l, rhoNOSg);
% lbm / in^3
            hg = table(Dome.density_E_g, Dome.enthalpy_E_g, rhoNOSg); %
BTU/lbm
            hl = table(Dome.density_E_g, Dome.enthalpy_E_l, rhoNOSg); %
BTU/lbm
            H = moxg*hg + moxl*hl;
            Ptc = (H - Utc) / Vt * (25037*12/32.2/32.2);
            dW = Ptc * dmox / rhoNOSl / 25037 * 32.2 / 12; % BTU / sec
%             dW = 0;
            dUt = -(dW + dmox*hl);  % BTU / sec
        else
            rhoNOSg = moxg / Vt;
            dmoxg = -dmox;
            dmoxl = 0;
            hg = table(Dome.density_E_g, Dome.enthalpy_E_g, rhoNOSg); %
BTU/lbm
            H = moxg * hg;
            Ptc = (H - Utc) / Vt * (25037*12/32.2/32.2);
            dUt = -dmox*hg;
        end

        dy(1) = dUt;
```

```
        dy(4) = dmoxl;
        dy(5) = dmoxg; % lbm/sec

        %% Progress
        clc
        t
        dmn
        F
        I
        Pcc
        Ptc
        rp
        Rex
%         pause(1/32)
        progressbar(t/tburn,'Hybrid Simulator')
%         set(display,'XData',t,'YData',Ptc)
%         set(display2,'XData',t,'YData',Pcc)
    end

% Non-ODE Related Functions
    function T = GetTemp(OtoF)
        if OtoF <= .728
            T = 1768.8*OtoF + 510.33;
        elseif OtoF > 30
            T = ChamberTemp;
        else
            T = -7.3514*OtoF^2 - 311.15*OtoF + 5927.1;  % see excel:
ISP.xls
        end
%         if OtoF <= 2
%             T = 643.86*OtoF+510.33;
%         elseif OtoF > 30
%             T = ChamberTemp;
%         else
%             T = -33.102*OtoF+1828.2;  % see excel: ISP.xls
%         end
    end

    function Rex = ExitR(OtoF)
       Rex = 8.314472 / (OtoF*44.013 + 54.09) * (OtoF + 1); % kJ / g-K
%         Rex = 1000*0.0945*OtoF^(-0.737); % kJ / g-K
        Rex = Rex * 0.5 / 4.448 * 39.37 * 453.59237; % in-lb / lbm-R
    end

    function [value,isterminal,direction] = event(t,r)
       value = Ptc - Patm;
       isterminal = 1;
       direction = 0;
    end
end
```

Acknowledgments

The authors would like to thank the following for their contributions towards the project:

Matt O'Connor, for his contributions through research into the safe use of nitrous oxide..

Nick Marcotte & Kris Hauert, for their work in previous iterations and documentation of past efforts in research, design, and development toward completing this project; specifically in the areas of project management, fuel grain curing, and testing.

Allen Capatini for helping in the construction and test process.

Cody Thompson, for his help in manufacturing various components and managing and maintaining facilities for the safe use of this project.

The Cal Poly Space Systems Club, for supplying the hardware, materials, financial support, and the support of the members during manufacturing and testing.

References

[1]Alagic, Vedran, et al. *MaCH-SR1*. Senior Project, University of Colorado, Boulder, Boulder: University of Colorado, Boulder, 2006.
[2]American Society of Metals. *Metals Handbook, Vol 2. - Properties and Selection: Nonferrous Alloys and Special-Purpose Materials.* ASM International, 1990.
[3]Beer, Ferdinand Pierre, E. Russel Johnston, and John T. DeWolf. *Mechanics of Materials.* Boston: McGraw-Hill Higher Education, 2006.
[4]Chiaverini, Martin J, and Kenneth K Kuo. *Fundamentals of Hybrid Rocket Combustion and Propulsion.* Virginia: AIAA, 2007.
[5]ESDU International plc. *Thermophysical Properties of Nitrous Oxide.* EDSU 2006-04, www.esdu.com, EDSU, 1991.
[6]Huzel, Dieter K., and David H. Huang. *Modern Engineering For Design of Liquid Propellant Rocket Engines.* Washington D.C.: American Institute of Aeronautics and Astronautics, 1992.
[7]Lee, Tsong-Sheng, and A. Potapkin. *The Performance of a Hybrid Rocket with Swirl GOx Injection.* Novosibirsk, Russia: Institute of Theoretical and Applied Mechanics Institutskaya, 2002.
[8]Lefebvre, Arthur H. *Atomization and Sprays.* New York: Hemisphere Publishing Corp., 1989.
[9]Moran, Michael J, and Howard N Shapiro. *Fundamentals of Engineering Thermodynamics.* New York: Wily, 2000.
[10]Nakka, Richard. *Richard Nakka's Experimental Rocketry Web Site.* http://www.nakka-rocketry.net/paradigm.html (accessed 6 7, 2010).
[11]Sutton, George P, and Oscar Biblarz. *Rocket Propulsion Elements.* New York: John Wiley & Sons., 2001.
[12]Tripoli Rocketry Association. "www.tripoli.org." *Tripoli Research Safety Code.* January 2010. http://tripoli.org/LinkClick.aspx?fileticket=YnzHZzIyiPE%3d&tabid=86 (accessed 6 7, 2010).
[13]Zucrow, Maurice J., and Joe D. Hoffmann. *Gas Dynamics.* New York: Wiley, 1976.